

1
2
3
4
5
6
7
8
9
10
11
12
13
14
15
16
17
18
19

On constraining the strength of the terrestrial CO₂ fertilization effect in an Earth system model

V. K. Arora and J. F. Scinocca.

Canadian Centre for Climate Modelling and Analysis, Environment and Climate Change Canada,
University of Victoria, Victoria, B.C., V8W 2Y2, Canada

20 **Abstract**

21
22 Earth system models (ESMs) explicitly simulate the interactions between the physical climate
23 system components and biogeochemical cycles. Physical and biogeochemical aspects of ESMs
24 are routinely compared against their observation-based counterparts to assess model performance
25 and to evaluate how this performance is affected by ongoing model development. Here, we assess
26 the performance of version 4.2 of the Canadian Earth system model against four, land carbon
27 cycle focused, observation-based determinants of the global carbon cycle and the historical global
28 carbon budget over the 1850-2005 period. Our objective is to constrain the strength of the
29 terrestrial CO₂ fertilization effect which is known to be the most uncertain of all carbon cycle
30 feedbacks. The observation-based determinants include 1) globally-averaged atmospheric CO₂
31 concentration, 2) cumulative atmosphere-land CO₂ flux, 3) atmosphere-land CO₂ flux for the
32 decades of 1960s, 1970s, 1980s, 1990s and 2000s and 4) the amplitude of the globally-averaged
33 annual CO₂ cycle and its increase over the 1980 to 2005 period. The optimal simulation that
34 satisfies constraints imposed by the first three determinants yields a net primary productivity
35 (NPP) increase from ~58 Pg C/yr in 1850 to about ~74 Pg C/yr in 2005; an increase of ~27% over
36 the 1850-2005 period. The simulated loss in the global soil carbon amount due to anthropogenic
37 land use change over the historical period is also broadly consistent with empirical estimates. Yet,
38 it remains possible that these determinants of the global carbon cycle are insufficient to
39 adequately constrain the historical carbon budget, and consequently the strength of terrestrial CO₂
40 fertilization effect as it is represented in the model, given the large uncertainty associated with
41 LUC emissions over the historical period.

42

43 **1. Introduction**

44

45 The evolution of the atmospheric CO₂ concentration in response to anthropogenic fossil fuel CO₂
46 emissions is determined by the rate at which a fraction of these emissions is taken up by the land
47 and ocean. Had the land and ocean not provided this “ecosystem service” since the start of the
48 industrial era, and not removed about 50% of CO₂ emissions from the atmosphere (Knorr, 2009),
49 the present concentration of CO₂ in the atmosphere would have been around 500 ppm, compared
50 to its current value of around 400 ppm. Over land, temperate and boreal forests as well as forests
51 in the tropical region are known to be sinks of atmospheric carbon (Ciais et al., 2013; Gourdji et
52 al., 2012; Schimel et al., 2015). The sink in the tropical forests is, however, compensated by
53 anthropogenic land use change emissions (Phillips and Lewis, 2014). Over ocean, the uptake of
54 anthropogenic carbon is observed to be larger in the high latitudes than in the tropical and
55 subtropical regions (Khatiwala et al., 2009). The manner in which the land and ocean will
56 continue to provide this ecosystem service in future is of both scientific and policy relevance.

57

58 Future projections of atmospheric CO₂ concentration, [CO₂], in response to continued
59 anthropogenic CO₂ emissions, or alternatively projections of CO₂ emissions compatible with a
60 given future [CO₂] pathway, are based primarily on comprehensive Earth system models (ESMs)
61 which include interactive land and ocean carbon cycle components (Jones et al., 2013). The land
62 and ocean carbon cycle components in ESMs respond both to increases in [CO₂] as well as the
63 associated changes in climate. These carbon components also respond to changes in climate
64 associated with other forcings including changes in concentration of non-CO₂ greenhouse gases
65 and aerosols, to nitrogen deposition and over land to anthropogenic land use change (LUC).

66

67 The response of land and ocean carbon cycle components to changes in [CO₂] and the associated
68 change in climate is most simply characterized in the framework of the 140-year long 1% per year
69 increasing CO₂ (1pctCO₂) experiment, in which [CO₂] increases at a rate of 1% per year from
70 pre-industrial value of about 285 ppm until concentration quadruples to about 1140 ppm. The
71 1pctCO₂ experiment has been recognized as a standard experiment by the coupled model
72 intercomparison project (CMIP) which serves to quantify the response of several climate and
73 Earth system metrics to increasing CO₂. These metrics include the transient climate response
74 (TCR) and the transient climate response to cumulative emissions (TCRE, Gillett et al., 2013).
75 Arora et al. (2013) analyzed results from fully-, biogeochemically- and radiatively-coupled
76 versions of the 1pctCO₂ experiment from eight ESMs that participated in the phase five of the
77 CMIP (CMIP5). They calculated the response of land and ocean carbon cycle components to
78 changes in [CO₂] and the associated change in climate expressed in terms of carbon-concentration
79 and carbon-climate feedbacks, respectively. Arora et al. (2013) found that of all the carbon cycle
80 feedbacks, the carbon-concentration feedback over land, which is primarily determined by the
81 strength of the terrestrial CO₂ fertilization effect, is the most uncertain across models. They found
82 that while the uncertainty in the carbon-concentration feedback over land (expressed in terms of
83 the standard deviation of the magnitude of the feedbacks) had somewhat reduced since the first
84 coupled carbon cycle climate model intercomparison project (C⁴MIP) (Friedlingstein et al., 2006)
85 its uncertainty remained the largest of all carbon cycle feedbacks. The comparison of the actual
86 magnitudes of the carbon cycle feedbacks over land is, however, not straightforward between the
87 Arora et al. (2013) and Friedlingstein et al. (2006) studies because they used different CO₂
88 scenarios.

89

90 The reason for this large uncertainty is that it is fairly difficult at present to constrain the strength
91 of the terrestrial CO₂ fertilization effect at the global scale. The net atmosphere-land CO₂ flux
92 since the start of the industrial era has not only been influenced by the changes in [CO₂] but also
93 the associated change in climate (due both to changes in [CO₂] and other climate forcings),
94 nitrogen deposition, and more importantly land use change - the contribution of which itself
95 remains highly uncertain. Since it is difficult to estimate the observed magnitude of net
96 atmosphere-land CO₂ flux since the start of the industrial era attributable only to increase in
97 [CO₂] it is consequently difficult to estimate the strength of the terrestrial CO₂ fertilization effect.

98
99 Measurements at Free-Air CO₂ Enrichment (FACE) sites in which vegetation is exposed to
100 elevated levels of [CO₂] help to assess some aspects of CO₂ fertilization and how nutrients
101 constraints regulate photosynthesis at elevated [CO₂] (Medlyn et al., 1999; McGuire et al., 1995).
102 However, FACE results cannot be easily extrapolated to the global scale and the response of
103 vegetation corresponds to a step increase in [CO₂] not the gradual increase which the real world
104 vegetation is experiencing.

105
106 As part of the ongoing evaluation of carbon cycle in ESMs, the model simulated aspects of the
107 global carbon cycle are routinely evaluated against their observation-based counterparts. These
108 evaluations also provide the opportunity to adjust physical processes that influence the strength of
109 the terrestrial CO₂ fertilization effect to provide the best comparison with observation-based
110 aspects of the global carbon cycle. Here, we present results from such an evaluation for a new
111 version of the Canadian Earth system model (CanESM4.2). An earlier version of the Canadian
112 Earth system model (CanESM2, Arora et al., 2011) participated in the CMIP5 (Taylor et al. 2012)

113 and its results also contributed to the fifth assessment report (AR5) of the Intergovernmental
114 Panel on Climate Change (IPCC). We evaluate the response of CanESM4.2, for three different
115 strengths of the terrestrial CO₂ fertilization effect, against four observation-based determinants of
116 the global carbon cycle and the historical global carbon budget over the 1850-2005 period, with a
117 focus on the land carbon cycle component. These determinants include 1) globally-averaged
118 atmospheric CO₂ concentration, 2) cumulative atmosphere-land CO₂ flux, 3) atmosphere-land
119 CO₂ flux for the decades of 1960s, 1970s, 1980s, 1990s and 2000s, and 4) the amplitude of the
120 globally-averaged annual CO₂ cycle and its increase over the 1980 to 2005 period.

121
122 The strength of the CO₂ fertilization effect influences all four of these determinants of the global
123 carbon cycle and the historical carbon budget. A stronger CO₂ fertilization effect, of course,
124 implies a larger carbon uptake by land and consequently a lower rate of increase of [CO₂] in
125 response to anthropogenic fossil fuel emissions. However, the strength of the CO₂ fertilization
126 effect also influences the amplitude of the annual [CO₂] cycle which is primarily controlled by the
127 northern hemisphere's biospheric activity. The amplitude of the annual [CO₂] cycle has been
128 observed to increase over the past five decades suggesting a gradual increase in photosynthesis in
129 association with a strengthening of the CO₂ fertilization effect (Keeling et al., 1996 ; Randerson et
130 al., 1997) and thus possibly can help to constrain the strength of the terrestrial CO₂ fertilization
131 effect in Earth system models.

132

133 **2. The coupled climate-carbon system and CanESM4.2**

134

135 **2.1 The coupled climate-carbon system**

136

137 The globally-averaged and vertically-integrated carbon budget for the combined atmosphere-
 138 land-ocean system may be written as:

$$139 \frac{dH_G}{dt} = \frac{dH_A}{dt} + \frac{dH_L}{dt} + \frac{dH_O}{dt} = E_F \quad (1)$$

141 where the Global carbon pool $H_G = H_A + H_L + H_O$ is the sum of carbon in the Atmosphere, Land
 142 and Ocean components, respectively (Pg C), and E_F is the rate of anthropogenic CO₂ emissions
 143 (Pg C/yr) into the atmosphere. The equations for the atmosphere, land and ocean components are
 144 written as

$$146 \begin{aligned} \frac{dH_A}{dt} &= F_A + E_F \\ &= -F_L - F_O + E_F \\ &= -(F_l - E_L) - F_O + E_F \\ &= -F_l - F_O + E_F + E_L \end{aligned} \quad (2)$$

$$\frac{dH_L}{dt} = F_L = F_l - E_L$$

$$\frac{dH_O}{dt} = F_O$$

148 where $(F_L + F_O) = -F_A$ are the fluxes (Pg C/yr) between the atmosphere and the underlying land
 149 and ocean, taken to be positive into the components. The net atmosphere-land CO₂ flux
 150 $F_L = F_l - E_L$ is composed of LUC emission rate E_L (Pg C/yr) as well as the remaining global
 151 “natural” CO₂ flux F_l that is often referred to as the residual or missing land sink in the context of
 152 the historical carbon budget (Le Quéré et al., 2015). The emissions associated with LUC occur
 153 when natural vegetation, for example, is deforested and replaced by croplands resulting in net loss
 154 of carbon from land to the atmosphere (i.e. positive E_L). Conversely, when croplands are
 155

156 abandoned and gradually replaced by forests then carbon is gained from atmosphere into the land
 157 (i.e. negative E_L).

158
 159 Over land, the rate of change of carbon is reflected in the model's three land pools (vegetation, V ;
 160 soil, S ; and litter or detritus, D)

$$\begin{aligned}
 \frac{dH_L}{dt} &= F_L = F_l - E_L \\
 &= \frac{dH_V}{dt} + \frac{dH_S}{dt} + \frac{dH_D}{dt} \\
 &= (G - R_A) - R_H - E_L \\
 &= N - R_H - E_L
 \end{aligned}
 \tag{3}$$

162 where G is the gross primary productivity (Pg C/yr) which represents the rate of carbon uptake by
 163 vegetation through photosynthesis, and R_A and R_H are the autotrophic and heterotrophic
 164 respiratory fluxes (Pg C/yr) from living vegetation and dead litter and soil carbon pools,
 165 respectively. $N = G - R_A$ is the net primary productivity (NPP) which represents the carbon
 166 uptake by vegetation after autotrophic respiratory costs have been taken into account. The
 167 heterotrophic respiration $R_H = R_{H,D} + R_{H,S}$ is composed of respiration from the litter and soil
 168 carbon pools. The rate of change in carbon in model's litter (H_D) and soil (H_S) pools is written as

$$\begin{aligned}
 \frac{dH_D}{dt} &= D_L + D_S + D_R - C_{D \rightarrow S} - R_{H,D} \\
 \frac{dH_S}{dt} &= C_{D \rightarrow S} - R_{H,S}
 \end{aligned}
 \tag{4}$$

170 where $D_{i,i=L,S,R}$ is the litter fall from the model's Leaf, Stem and Root components into the
 171 model's litter pool. $C_{D \rightarrow S}$ is the transfer of humidified litter into the soil carbon pool calculated as
 172 a fraction of the litter respiration ($R_{H,D}$)

$$C_{D \rightarrow S} = \chi R_{H,D}
 \tag{5}$$

174 and χ is the humification factor.

175

176 Integrating (2) and (3) in time with $\int_{t_0}^t (dH/dt)dt = H(t) - H(t_0) = \Delta H(t)$ and $\int_{t_0}^t F dt = \tilde{F}(t)$ (Pg

177 C) gives

$$\begin{aligned}\Delta H_A &= -(\tilde{F}_O + \tilde{F}_l) + (\tilde{E}_F + \tilde{E}_L) \\ \Delta H_O &= \tilde{F}_O \\ \Delta H_L &= \tilde{F}_L = \tilde{F}_l - \tilde{E}_L; \\ &= \Delta H_V + \Delta H_S + \Delta H_D = \tilde{F}_l - \tilde{E}_L = \tilde{N} - \tilde{R}_H - \tilde{E}_L \\ \Delta H_l &= \tilde{F}_l \\ \Delta H &= \tilde{E}_F\end{aligned}\tag{6}$$

179 The cumulative change in the atmosphere, the ocean and the land carbon pools is written as

$$\begin{aligned}\Delta H_A + \Delta H_O + (\Delta H_l - \tilde{E}_L) &= \tilde{E}_F \\ \Delta H_A + \Delta H_O + \Delta H_l &= \tilde{E}_F + \tilde{E}_L = \tilde{E}\end{aligned}\tag{7}$$

181 where \tilde{E} (Pg C) is the cumulative sum of the anthropogenic emissions from fossil fuel
182 consumption and land use change. When emissions associated with LUC are zero, equation (7)
183 becomes

$$\Delta H_A + \Delta H_O + \Delta H_L = \tilde{E}_F = \tilde{E}\tag{8}$$

185 which indicates how cumulative emissions are parsed into changes in atmospheric carbon burden
186 and carbon uptake by the ocean and land components.

187

188 **2.2 Canadian Earth System Model version 4.2**

189

190 **2.2.1 Physical components**

191
192 At the Canadian Centre for Climate Modelling and Analysis (CCCma), the earth system model,
193 CanESM2, has undergone further development since its use for CMIP5. This version of the
194 model has been equivalently labelled CanESM4.0 in an effort to rationalize the ESM naming
195 convention to better reflect the fact that this model version employs the 4th generation atmosphere
196 component, CanAM4, (Von Salzen et al. 2013) and the 4th generation ocean component, CanOM4
197 (Arora et al., 2011). The version of the CCCma earth system model used for this study is
198 CanESM4.2 and so, represents two full cycles of model development on all of its components.
199 Similar to CanESM2, the physical ocean component of CanESM4.2 (CanOM4.2) has 40 levels
200 with approximately 10 m resolution in the upper ocean while the horizontal ocean resolution is
201 approximately 1.41° (longitude) \times 0.94° (latitude). The majority of development in CanESM4.2,
202 relative to CanESM2, has occurred on its atmospheric component CanAM4.2. CanAM4.2 is a
203 spectral model employing T63 triangular truncation with physical tendencies calculated on a 128
204 \times 64 ($\sim 2.81^\circ$) horizontal linear grid with 49 layers in the vertical whose thicknesses increase
205 monotonically with height to 1 hPa. Relative to CanAM4, CanAM4.2 includes a new version of
206 the Canadian Land Surface Scheme, CLASS3.6, which models the energy and water fluxes at the
207 atmosphere-land boundary by tracking energy and water through the soil, snow, and vegetation
208 canopy components (Verseghy, 2012). CLASS models the land surface energy and water balance
209 and calculates liquid and frozen soil moisture, and soil temperature for three soil layers (with
210 thicknesses 0.1, 0.25 and 3.75 m). The thickness of the third layer depends on the depth to
211 bedrock (and is in many places less than 3.75 m) based on the Zobler (1986) soil data set.
212 Changes to CLASS primarily include improvements to the simulation of snow at the land surface.
213 These incorporate new formulations for vegetation interception of snow (Bartlett et al., 2006), for

214 unloading of snow from vegetation (Hedstrom and Pomeroy, 1998), for the albedo of snow-
215 covered canopies (Bartlett and Verseghy, 2015), for limiting snow density as a function of depth
216 (Tabler et al., 1990; Brown et al., 2006), and for the thermal conductivity of snow (Sturm et al.,
217 1997). Water retention in snowpacks has also been incorporated. CanAM4.2 also includes an
218 aerosol microphysics scheme (von Salzen, 2006; Ma et al., 2008; Peng et al., 2012), a higher
219 vertical resolution in the upper troposphere, a reduced solar constant (1361W/m^2) and an
220 improved treatment of the solar continuum used in the radiative transfer. CanAM4.2 also
221 considers natural and anthropogenic aerosols and their emissions, transport, gas-phase and
222 aqueous-phase chemistry, and dry and wet deposition as summarized in Namazi et al. (2015)

223

224 **2.2.2 Land and ocean carbon cycle components**

225

226 The ocean and land carbon cycle components of CanESM4.2, are similar to CanESM2, and
227 represented by the Canadian Model of Ocean Carbon (CMOC) (Christian et al., 2010) and the
228 Canadian Terrestrial Ecosystem Model (CTEM) (Arora et al., 2009; Arora and Boer, 2010),
229 respectively.

230

231 LUC emissions in CTEM are modelled interactively on the basis of changes in land cover which
232 are determined by changes in crop area. The historical land cover used in the simulations
233 presented here is reconstructed using the linear approach of Arora and Boer (2010) and is the
234 same as used for CMIP5 simulations; as the fraction of crop area in a grid cell changes, the
235 fraction of non-crop plant functional types (PFTs) is adjusted linearly in proportion to their
236 existing coverage. The historical changes in crop area are based on the data set provided for

237 CMIP5 simulations as explained in Arora and Boer (2014). When the fraction of crop area in a
 238 grid cell increases then the fractional coverage of other PFTs is reduced which results in
 239 deforested biomass. The deforested biomass is allocated to three components that are i) burned
 240 instantaneously and contribute to ii) short (paper) and iii) long (wood products) term pools (Arora
 241 and Boer, 2010). The deforested biomass corresponding to paper and wood products is
 242 transferred to model's litter and soil carbon pools, respectively. When the fraction of crop area
 243 decreases, the fractional coverage of non-crop PFTs increases and their vegetation biomass is
 244 spread over a larger area reducing vegetation density. Carbon is sequestered until a new
 245 equilibrium is reached providing a carbon sink associated with regrowth as the abandoned areas
 246 revert back to natural vegetation.

247
 248 The LUC emissions term (E_L) in the equations (1) through (8) is not easily defined or calculated.
 249 Pongratz et al. (2014) discuss the multiple definitions and methods of calculating E_L . When E_L
 250 is calculated using models, it is most usually defined as the difference in F_L between simulations
 251 with and without LUC. This is also the basic definition used by Pongratz et al. (2014).
 252 Calculating E_L thus requires performing additional simulations without land use change in which
 253 land cover is held constant at its pre-industrial state. For a simulation without LUC equation (3)
 254 becomes

$$\frac{dH'_L}{dt} = F'_L = F'_I \quad (9)$$

256 and an estimate of E_L , and its cumulative values \tilde{E}_L , is obtained as

$$\begin{aligned} E_L &= F'_L - F_L \\ \tilde{E}_L &= \tilde{F}'_L - \tilde{F}_L \end{aligned} \quad (10)$$

258 Over the historical period, globally, F'_L is expected to be higher than F_L (both considered
259 positive downwards) due, at least, to two processes: 1) fraction of deforested biomass that is
260 burned and which contributes to short and long term product pools all release carbon to the
261 atmosphere, albeit at different time scales, 2) the area that is deforested and put under agricultural
262 use loses soil carbon and cannot sequester carbon in response to increase $[\text{CO}_2]$ since crops are
263 frequently harvested. As a result E_L is positive.

264
265 Relative to CanESM2, the version of CTEM employed in CanESM4.2, CTEM4.2, includes
266 changes to the humification factor (χ , see equations 4 and 5) which determines what fraction of
267 the humidified litter is transferred from litter (H_D) to the soil carbon pool (H_S). The value of χ
268 employed in CTEM4.2 has been changed for crop PFTs from 0.45 to 0.10, which decreases the
269 transfer of the humidified litter to the soil carbon pool. As a result, a decrease in global soil
270 carbon over the historical period is obtained as natural vegetation is replaced by croplands as is
271 seen in empirical measurements (Wei et al., 2014). This change in humification factor was
272 required despite the higher litter decomposition rates over croplands and is discussed in more
273 detail later in the results section. In addition, in CTEM4.2 the sensitivity of photosynthesis to soil
274 moisture is reduced for coupling to CLASS 3.6, especially for the broadleaf evergreen PFT
275 (which exists mainly in the tropics) to somewhat account for deep roots, for example, in the
276 Amazonian region (e.g. see da Rocha et al., 2004).

277
278 CTEM has always included a parameterization of photosynthesis down-regulation, which
279 represents acclimatization to elevated CO_2 in the form of a decline in maximum photosynthetic
280 rate. In the absence of explicit coupling of terrestrial carbon and nitrogen cycles this

281 parameterization yields a mechanism to reduce photosynthesis rates as [CO₂] increases. The
 282 photosynthesis down-regulation parameterization is described in detail in Arora et al. (2009) and
 283 is based on earlier simpler models which expressed net or gross primary productivity (NPP or
 284 GPP) as a logarithmic function of atmospheric CO₂ concentration (e.g. Cao et al., 2001;
 285 Alexandrov and Oikawa, 2002).

$$286 \quad G(t) = G_0 \left(1 + \gamma_p \ln \left(\frac{C(t)}{C_0} \right) \right) \quad (11)$$

287 where GPP at any given time, $G(t)$, is a function of its initial value G_0 , atmospheric CO₂
 288 concentration at time t , $C(t)$, and its initial value C_0 . The rate of increase of GPP is determined by
 289 the parameter γ_p (where p indicates the “potential” rate of increase of GPP with CO₂). The ratio
 290 of GPP in two different versions of a model in which GPP increases at different rates (γ_p and γ_d)
 291 is given by

$$292 \quad \xi(C) = \frac{1 + \gamma_d \ln(C/C_0)}{1 + \gamma_p \ln(C/C_0)} \quad (12)$$

293
 294 where t is omitted for clarity. When $\gamma_d < \gamma_p$, the modelled potential gross photosynthesis rate
 295 (G_p), which is not constrained by nutrient limitation, can be multiplied by the scalar $\xi(C)$
 296 (equation 12) which yields the gross primary productivity (G) used in equation (3) that now
 297 increases in response to CO₂ increases at a rate determined by the value of γ_d (the subscript d
 298 indicates down-regulation).

$$299 \quad G = \xi(C) G_p \quad (13)$$

300

301 A lower value of γ_d than γ_p yields a value of $\xi(C)$ that is less than one. As the concentration of
302 CO_2 , expressed as C in equation (12), increases above its pre-industrial level C_0 (285 ppm), $\xi(C)$
303 progressively decreases resulting in a gross primary productivity G , which is less than the its
304 potential value G_p . Figure 1 shows the behaviour of $\xi(C)$ for $\gamma_p=0.95$ and three values of γ_d
305 (0.25, 0.4 and 0.55) corresponding to three different strengths of the terrestrial CO_2 fertilization
306 effect. A value of $\gamma_d = 0.25$ was used for CanESM2 to best simulate the globally-averaged
307 surface CO_2 concentration and cumulative 1850-2005 atmosphere-land CO_2 flux. CanESM2,
308 however, wasn't as rigorously evaluated as we have attempted here for CanESM4.2. Through
309 the parameter γ_d , the physical process of down-regulation has a direct influence on the strength
310 of the terrestrial CO_2 fertilization effect. In practice, different combinations of γ_d and γ_p are able
311 to yield very similar values of $\xi(C)$. Arora et al. (2009) calculated the value of γ_d based on
312 results from six studies, two of which were meta-analyses each based on 15 and 77 individual
313 studies, that grow plants in ambient and elevated CO_2 environment. Their results are equivalent to
314 $\gamma_d=0.46$ with a range from 0.22 to 0.63 for $\gamma_p=0.95$.

315
316 In Figure 1, while $\xi(C)$ decreases with an increase in atmospheric CO_2 , indicating progressive
317 decline in photosynthesis due to nutrient limitation, the slope $\frac{d\xi}{dC}$ also decreases. Although a
318 second-order effect, this is a limitation of the current formulation of $\xi(C)$. A decreasing $\xi(C)$ as
319 CO_2 increases can eventually also lead to decrease in GPP although we have not seen this
320 behaviour up to CO_2 concentration of around 1000 ppm in simulations performed with CanESM2
321 (see Arora and Boer, 2014). While γ_d is used to model down-regulation of photosynthesis it may

322 also be used as a measure of the strength of the CO₂ fertilization effect. Lower values of γ_d
323 indicate higher down-regulation (see Figure 1) so higher values of γ_d imply higher strength of the
324 CO₂ fertilization effect. Finally, γ_d is specific to CTEM and as such the value of this parameter is
325 irrelevant to other models. More relevant for comparison with other models is the simulated rate
326 of increase of NPP over the historical period that a given value of γ_d yields.

327

328 **2.2.3 Treatment of CO₂ in the atmosphere**

329

330 The land and ocean components of the carbon cycle in CanESM4.2 are operable for two
331 experimental designs – 1) an emissions-driven mode, where the atmospheric CO₂ concentration is
332 a freely evolving 3D tracer in the model and 2) a concentrations-driven mode, where the
333 atmospheric CO₂ concentration is prescribed externally.

334

335 In the emissions-driven mode the anthropogenic CO₂ emissions (E_F) are specified and since the
336 interactive land and ocean carbon cycle components simulate the F_L and F_O terms, respectively,
337 the model is able to simulate the evolution of [CO₂] through the H_A term, which represents the
338 atmospheric carbon burden, in equation (2). This is referred to as the interactively simulated
339 [CO₂], or “free-CO₂” configuration. In this case, the model simulates the transport of CO₂ in the
340 atmosphere producing 3D structure, an annual cycle, and inter-annual variability.

341

342 In the concentrations-driven mode, the land and ocean CO₂ fluxes, F_L and F_O , remain
343 interactively determined so model results can be used to diagnose the E_F term (based on equation
344 2) that is compatible with a given [CO₂] pathway at the global scale. The concentrations-driven

345 mode can be executed in two CanESM4.2 configurations. In the first configuration, a single scalar
346 value of $[\text{CO}_2]$, which may be time evolving, is imposed at all geographical and vertical locations
347 in the model. This follows the CMIP5 prescription for concentrations-driven simulations and we
348 refer to it here as, “specified-CO2” concentrations-driven mode. In the second configuration, a
349 new approach for specifying CO_2 concentration has been implemented in CanESM4.2. In this
350 new approach, only the globally averaged concentration of CO_2 in the lowest model level is
351 constrained by the prescribed value. The geographical and vertical distribution of CO_2 in the
352 atmosphere and its annual cycle in this second configuration is otherwise free to evolve in the
353 same manner as in the emissions-driven, free-CO2, configuration. A relaxation timescale of one
354 day is employed in this new configuration and a fixed annual cycle, derived from the free-CO2
355 preindustrial control simulation, is imposed on the reference value of $[\text{CO}_2]$. The reference value
356 of $[\text{CO}_2]$ may additionally be specified as time evolving. We refer to this configuration as the
357 “relaxed-CO2” concentrations-driven mode. Aside from the relaxational constraint on the global-
358 mean surface value of $[\text{CO}_2]$, the atmospheric configuration for relaxed-CO2 is identical to that
359 for free-CO2 with zero emissions. As a consequence, the relaxed CO2 configuration allows the
360 same nonlinearity in the atmosphere-surface exchange of CO_2 as the free CO2 configuration
361 leading to nearly identical spatial distribution and seasonal cycle of atmosphere CO_2
362 concentrations. In this regard, the relaxed-CO2 configuration is physically more realistic than the
363 specified-CO2 configuration.

364
365 There are practical advantages to using the relaxed-CO2 configuration over the specified-CO2
366 configuration for concentrations-driven simulations. When spinning up land and ocean carbon
367 pools in a preindustrial control simulation, the model is executed in concentrations driven mode

368 to bring these pools into equilibrium with a prescribed CO₂ concentration. In earlier versions of
369 the CanESM, a specified-CO₂ configuration was used for this purpose. Beginning with version
370 4.1, the relaxed-CO₂ configuration is used for this purpose because it produces little or no drift
371 when used to initialize the free-CO₂ preindustrial control simulations. In fact, a relaxed-CO₂
372 preindustrial control simulation may be used as the control simulation for both emissions-driven
373 and (relaxed-CO₂) concentrations-driven experiments. This is not the case when the specified-
374 CO₂ is used as the configuration for concentration driven experiments.

375

376 **3. Experimental set up**

377

378 Three different kinds of experiments are performed for this study. The first is the standard 1% per
379 year increasing CO₂ experiment (1pctCO₂) performed for three different strengths of the
380 terrestrial CO₂ fertilization effect. The 1pctCO₂ is a concentration-driven experiment and we use
381 the “relaxed-CO₂” configuration to specify CO₂ in the atmosphere. The second experiment is the
382 CMIP5 1850-2005 historical experiment, referred to as esmhistorical following CMIP5
383 terminology, which is performed with specified anthropogenic CO₂ emissions (i.e. in emissions-
384 driven, or “free-CO₂”, mode), where [CO₂] is simulated interactively. Concentrations of non-CO₂
385 greenhouse gases and emissions of aerosols and their precursors are specified in the esmhistorical
386 experiment following the CMIP5 protocol. The third experiment is same as the esmhistorical
387 experiment but LUC is not permitted and the land cover remains at its 1850 value; referred to as
388 the esmhistorical_noluc experiment. Two ensemble members are performed for each of the three
389 versions of the esmhistorical and esmhistorical_noluc experiments corresponding to three
390 different strengths of the terrestrial CO₂ fertilization effect. The rationale for performing historical

391 simulations without LUC is to be able to quantify LUC emissions E_L using equation (10). Table
392 1 summarizes all the simulations performed.

393
394 The 1pctCO2 simulations with “relaxed” CO₂ for three different strengths of the terrestrial CO₂
395 fertilization effect are initialized from a corresponding pre-industrial control simulation with CO₂
396 specified at ~285 ppm and all other forcings at their 1850 values. The esmhistorical and
397 esmhistorical_noluc simulations are initialized from a pre-industrial control simulation with
398 “free” CO₂ and zero anthropogenic CO₂ emissions.

399

400 **4. Results**

401

402 **4.1. 1% per year increasing CO₂ experiments**

403

404 Figure 2 shows the carbon budget components of equation (8); ΔH_A , ΔH_O and ΔH_L i.e. the
405 change in atmospheric carbon burden and cumulative atmosphere-ocean and atmosphere-land
406 CO₂ flux which together make up the cumulative diagnosed emissions (\tilde{E}) based on results from
407 the fully-coupled 1pctCO2 experiment. Results are shown from eight CMIP5 models that
408 participated in the Arora et al. (2013) study, including CanESM2 which used $\gamma_d=0.25$, together
409 with those from CanESM4.2 for three different strengths of the terrestrial CO₂ fertilization effect.

410 The cumulative atmosphere-land CO₂ flux across models varies much more than the cumulative
411 atmosphere-ocean CO₂ flux across the CMIP5 models as already noted in Arora et al. (2013). The
412 results for CanESM4.2 indicate that the influence of γ_d (equation 12) on the strength of the
413 model’s terrestrial CO₂ fertilization effect allows CanESM4.2’s cumulative diagnosed emissions
414 to essentially span the range of the other CMIP5 models. For the three different strengths of the

415 terrestrial CO₂ fertilization effect, $\gamma_d = 0.25, 0.4$ and 0.55 , the γ_d values of 0.4 and 0.55 yield
416 cumulative atmosphere-land CO₂ flux that is higher than all the CMIP5 models. The basis for
417 choosing these values of γ_d within the range 0.4 ± 0.15 is that they span the observation-based
418 estimates of various quantities reasonably well as shown later.

419

420 The cumulative atmosphere-land CO₂ flux ΔH_L for CanESM4.2 for the simulation with $\gamma_d=0.25$
421 is higher than that for CanESM2 which also uses $\gamma_d=0.25$, because of the changes made to soil
422 moisture sensitivity of photosynthesis and because ΔH_L also depends on the model climate. In
423 particular, the CanESM2 bias of low precipitation over the Amazonian region has been reduced
424 in CanESM4.2, as shown in Figure 3. The increased precipitation over the Amazonian region
425 causes increased carbon uptake with increasing [CO₂]. The improved precipitation bias of
426 CanESM4.2 in this region is in part caused by the decreased sensitivity of photosynthesis to soil
427 moisture in CTEM4.2, especially for broadleaf evergreen PFT, which helps to increase
428 evapotranspiration and in turn increase precipitation over the region.

429

430 **4.2. Historical simulations with LUC**

431

432 The results presented in this section evaluate the model against four observation-based
433 determinants of the global carbon cycle and the historical global carbon budget over the 1850-
434 2005 period mentioned earlier. Simulated atmosphere-ocean CO₂ fluxes are also compared with
435 observation-based estimates although, of course, they are not directly affected by the strength of
436 the terrestrial CO₂ fertilization effect.

437

438 **4.2.1. Components of land carbon budget**

439

440 In Figure 4, time series of instantaneous (F_L panel a) and cumulative (\tilde{F}_L panel b) atmosphere-
441 land CO₂ flux over the period 1850-2005 are displayed for CanESM2 (which contributed results
442 to CMIP5) and CanESM4.2 for the three different strengths of the terrestrial CO₂ fertilization
443 effect. The observation-based estimates of $F_L = (F_I - E_L)$ in Figure 4a for the decades of 1960,
444 1970, 1980, 1990 and 2000 are reproduced from Le Quéré et al. (2015) who derive the
445 $F_L = (F_I - E_L)$ term as residual of the carbon budget equation $dH_A/dt = -(F_I - E_L) - F_O + E_F$
446 using observation-based estimates of change in atmospheric carbon budget (dH_A/dt),
447 atmosphere-ocean CO₂ flux (F_O) and fossil fuel emissions (E_F). The observation-based estimate
448 of -11 ± 47 Pg C in Figure 4b for \tilde{F}_L over the period 1850-2005 is from Arora et al. (2011) (their
449 Table 1).

450

451 The primary difference between CanESM2 and CanESM4.2 simulations in Figure 4 is that \tilde{F}_L for
452 CanESM2 generally stays positive throughout the historical period, whereas for CanESM4.2 it
453 first becomes negative (indicating that land is losing carbon) and then becomes positive
454 (indicating that land is gaining carbon) towards the end of the 20th century, depending on the
455 strength of the CO₂ fertilization effect. The behaviour of \tilde{F}_L for CanESM4.2 is considered to be
456 more realistic. As the land responds to anthropogenic land use change, associated with an increase
457 in crop area early in the historical period, it causes a decrease in vegetation and soil carbon (see
458 Figure 5). Later in the 20th Century, the CO₂ fertilization effect causes the land to become a sink
459 for carbon resulting in both vegetation and soil carbon increases. This behavior is consistent with
460 the mean model response of the 15 CMIP5 models analyzed by Hoffman et al. (2013) (their

461 Figure 2b). In contrast, CanESM2 shows a gradual increase in the global soil carbon amount
462 (Figure 5a) over the historical period. In Figure 5, it can be seen that the effect of CO₂ fertilization
463 in the second half of the 20th century is delayed for soil carbon compared to that for vegetation.
464 This is primarily because of the lag introduced by the turnover time of vegetation (i.e., increased
465 NPP inputs have to go through vegetation pool first) and the longer turnover time scale of the soil
466 carbon pool. The more reasonable response of soil carbon to anthropogenic land use change, in
467 Figure 5a for CanESM4.2, is achieved by changing the humification factor from 0.45 (in
468 CanESM2) to 0.10 (in CanESM4.2) in equation (5) which yields a reduction in global soil carbon
469 amount in response to land use change up until the time that the effect of CO₂ fertilization starts
470 to take effect. In Figure 4a, CanESM4.2 is also able to simulate continuously increasing F_L during
471 the period 1960 to 2005, depending on the strength of the CO₂ fertilization effect, while
472 CanESM2 simulates near constant or decreasing F_L from about 1990 onwards, as is also seen in
473 Figure 4b for \tilde{F}_L . This behaviour of F_L is not consistent with observation-based estimates from
474 Le Quéré et al. (2015) which show continued strengthening of the land carbon sink since 1960s.

475
476 In Figure 4a, amongst the three versions of the CanESM4.2, the simulation with $\gamma_d = 0.4$ (blue
477 line) yields the best comparison with observation-based estimates of F_L from Le Quéré et al.
478 (2015), while the simulations with $\gamma_d = 0.25$ (green line) and $\gamma_d = 0.55$ (red line) yield F_L values
479 that are lower and higher, respectively, than observation-based estimates. In Figure 4b, the
480 cumulative atmosphere-land CO₂ flux \tilde{F}_L over the 1850-2005 period from the simulations with
481 $\gamma_d = 0.25$ and 0.4 (green and blue lines, respectively) lies within the uncertainty of observation-

482 based estimates, while the simulation with $\gamma_d = 0.55$ (red line) yields \tilde{F}_L value that is high
483 relative to observation-based estimate.

484
485 Figure 6 shows the change in and absolute values of NPP from CanESM2 and the simulations
486 made with CanESM4.2 for three different strengths of the CO₂ fertilization effect. Consistent with
487 1pctCO2 simulations, the rate of increase of NPP in CanESM4.2 with $\gamma_d = 0.25$ is higher than
488 that in CanESM2 which also uses $\gamma_d = 0.25$. This is because the underlying model climate is
489 different in CanESM2 and CanESM4.2, as mentioned earlier, and the fact that photosynthesis
490 sensitivity to soil moisture has also been reduced. The rates of increase of NPP for $\gamma_d = 0.40$ and
491 0.50 are, of course, even higher. The CanESM4.2 simulation with $\gamma_d = 0.40$, which yields the
492 best comparison with observation-based estimates of F_L for the decade of 1960 through 2000
493 (Figure 4a) as well as \tilde{F}_L for the period 1850-2005 (Figure 4b), yields an increase in NPP of ~16
494 Pg C/yr over the 1850-2005 period. A caveat here is that part of this increase is also caused by
495 increase in the crop area over the historical period that is realized in the model regardless of the
496 strength of the CO₂ fertilization effect. In CTEM, the maximum photosynthetic capacity of crops
497 is higher than for other PFTs to account for the fact that agricultural areas are generally fertilized.
498 As a result, increase in crop area also increases global NPP. The increasing crop productivity has
499 been suggested to contribute to the increase in amplitude of the annual [CO₂] cycle since 1960s
500 (Zeng et al., 2014). However, in the absence of an explicit representation of terrestrial N cycle
501 (and thus fertilization of cropped areas) or a representation of increase in crop yield per unit area
502 due to genetic modifications, the only processes in CTEM that contribute to changes in crop yield
503 are the change in crop area itself and the increase in crop NPP due to the CO₂ fertilization effect.

504

505 **4.2.2. Globally-averaged [CO₂]**

506

507 Figure 7 shows the simulated globally-averaged surface [CO₂] from the emissions-driven
508 esmhistorical simulation of CanESM2 and that of CanESM4.2 for three different strengths of the
509 CO₂ fertilization effect. The observation-based time series of [CO₂] is illustrated by the heavy
510 black line. The CanESM2 ($\gamma_d=0.25$) simulation yields a reasonable comparison with observation-
511 based [CO₂]. Amongst the versions of CanESM4.2 with different strengths of the CO₂
512 fertilization effect, the version with $\gamma_d=0.40$ yield the best comparison. The CanESM4.2 version
513 with $\gamma_d=0.25$ (weaker strength of the CO₂ fertilization effect) and 0.55 (stronger CO₂ fertilization
514 effect) yield CO₂ concentrations that are respectively higher and lower than the observational
515 estimate from roughly mid-20th Century onward. The reason CanESM4.2 ($\gamma_d=0.40$) requires a
516 stronger CO₂ fertilization effect than CanESM2 ($\gamma_d=0.25$) for simulating the observation-based
517 increase in atmospheric CO₂ burden over the historical period is the enhanced impact of LUC in
518 CanESM4.2 due to its increased humification factor and the associated response of the global soil
519 carbon pool, as discussed in the previous section. The differences in simulated [CO₂] in Figure 7
520 from CanESM4.2 are due only to differences in the strength of the CO₂ fertilization effect.
521 Although, of course, since in these simulations [CO₂] is simulated interactively, the simulated
522 atmosphere-land flux F_L and [CO₂] both respond to and affect each other.

523

524 Both CanESM2 and CanESM4.2 underpredict [CO₂] relative to observational estimates over the
525 period 1850-1930, and are also unable to reproduce the near zero rate of increase of [CO₂] around
526 1940. Possible reasons for these discrepancies include 1) the possibility that carbon cycle before

527 1850 was not in true equilibrium and this aspect cannot be captured since the model is spun up to
528 equilibrium for 1850 conditions, 2) the uncertainties associated with anthropogenic emissions for
529 the late 19th and early 20th century that are used to drive the model, and 3) the uncertainties
530 associated with pre Mauna-Loa [CO₂] observations.

531

532 **4.2.3. Atmosphere-ocean CO₂ flux**

533

534 Figures 8a and b, respectively, show time series of instantaneous (F_o) and cumulative (\tilde{F}_o)
535 atmosphere-ocean CO₂ fluxes over the period 1850-2005 for the set of emissions-driven
536 simulations presented in Fig. 7. The strength of the terrestrial CO₂ fertilization effect has little or
537 no impact on the ocean biogeochemical processes. The differences in values of F_o and \tilde{F}_o for
538 the three versions CanESM4.2 are, therefore, primarily due to the differences in [CO₂]. The
539 observation-based estimates of F_o in Figure 8a for the decades of 1960, 1970, 1980, 1990 and
540 2000 are from Le Quéré et al. (2015). The observation-based estimate of \tilde{F}_o of 141±27 Pg C in
541 Figure 8b for the period 1850-2005 is from Arora et al. (2011) (their Table 1).

542

543 Both CanESM2 and the CanESM4.2 simulation for $\gamma_d=0.40$ (which provides the best comparison
544 with observation-based estimate for [CO₂]; blue line in Figure 7) yield lower \tilde{F}_o compared to
545 observation-based values. The F_o value from CanESM2 and the CanESM4.2 simulation for
546 $\gamma_d=0.40$ are lower than the mean estimates from Le Quéré et al. (2015) for the decades of 1960s
547 through 2000s, although still within their uncertainty range. The family of ESMs from CCCma,
548 all of which have the same physical ocean model, including CanESM1 (Arora et al., 2009),

549 CanESM2 (Arora et al., 2011) and now CanESM4.2, yield lower than observed ocean carbon
550 uptake over the historical period. Recent analyses of these model versions suggest that the
551 primary reason for their low carbon uptake is a negative bias in near surface wind speeds over the
552 Southern Ocean and an iron limitation in the same region which is too strong (personal
553 communication, Dr. Neil Swart, Canadian Centre for Climate Modelling and Analysis). The
554 CanESM4.2 simulation with $\gamma_d=0.25$ (green line in Figure 8) yields a better comparison with
555 observation-based estimates of F_o and \tilde{F}_o but that is because of the higher simulated $[\text{CO}_2]$ in
556 that simulation associated with lower carbon uptake by land.

557

558 **4.2.4. Amplitude of the annual CO₂ cycle**

559

560 The annual CO₂ cycle is influenced strongly by the terrestrial biospheric activity of the northern
561 hemisphere (Keeling et al., 1996; Randerson et al., 1997). Higher than normal biospheric uptake
562 of carbon during a northern hemisphere's growing season, for example, will yield lower than
563 normal $[\text{CO}_2]$ by the end of the growing season, around September when $[\text{CO}_2]$ is at its lowest
564 level (see Figure 9a). Similarly, during the northern hemisphere's dormant season, increased
565 respiration from live vegetation and decomposition of dead carbon, including leaf litter, that may
566 be associated with increased carbon uptake during the last growing season, will yield higher than
567 normal $[\text{CO}_2]$ during April when $[\text{CO}_2]$ is at its highest level. Both processes increase the
568 amplitude of the annual $[\text{CO}_2]$ cycle. Given this strong control, the rate of change of the
569 amplitude of the annual $[\text{CO}_2]$ cycle can potentially help to constrain the strength of the terrestrial
570 CO₂ fertilization effect.

571

572 Figure 9a compares the annual cycle of the trend-adjusted globally-averaged near-surface
573 monthly [CO₂] anomalies from CanESM2 and the versions of CanESM4.2 for three different
574 strengths of the CO₂ fertilization effect with observation-based estimates for the 1991-2000
575 period. Figure 9b shows the time series of the amplitude of the annual cycle of the trend adjusted
576 globally-averaged near-surface monthly [CO₂] anomalies (referred to as Φ_{CO_2}) from CanESM2
577 and CanEM4.2, as well as observation-based estimates going back to 1980s. While CO₂
578 measurements at Mauna Loa started in 1959, observation-based globally-averaged near-surface
579 [CO₂] values are only available since 1980s
580 (ftp://aftp.cmdl.noaa.gov/products/trends/co2/co2_mm_gl.txt). In Figure 9b, consistent with the
581 strengthening of the CO₂ fertilization effect, associated with the increase in [CO₂], the
582 observation-based estimate of Φ_{CO_2} shows an increase from 1980s to the present. Both CanESM2
583 and versions of CanESM4.2 also show an increase in the amplitude of Φ_{CO_2} over the period
584 1850-2005. However, the absolute values of Φ_{CO_2} are lower in CanESM2 than in CanESM4.2
585 (Figure 9b). Of course, in the absence of an observation-based estimate of pre-industrial value of
586 Φ_{CO_2} it is difficult to say which value is more correct. However, when considering the present
587 day values of Φ_{CO_2} the three versions of CanESM4.2 yield better comparison with observation-
588 based estimate as also shown in Figure 9a. The increase in the value of Φ_{CO_2} from CanESM2 to
589 CanESM4.2, which now yields better comparison with observation-based value of Φ_{CO_2} , is most
590 likely caused by the change in the land surface scheme from CLASS 2.7 (that is implemented in
591 CanESM2) to CLASS 3.6 (implemented in CanESM4.2), since the atmospheric component of the
592 model hasn't changed substantially. It is, however, difficult to attribute the cause of this
593 improvement in the present day value of Φ_{CO_2} in CanESM4.2 to a particular aspect of the new

594 version of the land surface scheme. The annual [CO₂] cycle is driven primarily by the response of
595 the terrestrial biosphere to the annual cycle of temperature and the associated greening of the
596 biosphere every summer in the northern hemisphere. However, the simulated amplitude of the
597 annual cycle of near-surface temperature hasn't changed substantially from CanESM2 to
598 CanESM4.2 (not shown).

599
600 In Figure 9b, the simulated values of Φ_{CO_2} for the CanESM4.2 simulations with $\gamma_d=0.25, 0.40$
601 and 0.55 are $4.41, 4.69$ and 4.85 ppm, respectively, averaged over the period 1991-2000,
602 compared to observation-based value of Φ_{CO_2} of 4.36 ppm. Here, CanESM4.2 simulation with
603 $\gamma_d=0.25$ yields the best comparison with observation-based value of Φ_{CO_2} . An increase in the
604 strength of the CO₂ fertilization effect increases the amplitude of the annual [CO₂] cycle so a
605 larger value of γ_d yields a larger value of Φ_{CO_2} . The increase in the amplitude of the annual
606 [CO₂] cycle comes both from lower [CO₂] at the end of the growing season in September as well
607 as higher [CO₂] at the start of the northern hemisphere's growing season in April (see Figure 9a),
608 as mentioned earlier in this section.

609
610 More important than the absolute value of Φ_{CO_2} is its rate of increase over time which is a
611 measure of the strength of the terrestrial CO₂ fertilization effect. Figure 9b also shows the trend in
612 Φ_{CO_2} over the 1980-2005 overlapping period for which for both the model and observation-based
613 estimates of Φ_{CO_2} are available. The magnitude of trend for observation-based estimate of Φ_{CO_2}
614 is 0.142 ± 0.08 ppm/10-years (mean \pm standard deviation, $\bar{x} \pm \sigma_x$), implying that over the 26 year
615 1980-2005 period the amplitude of annual [CO₂] cycle has increased by 0.37 ± 0.21 ppm. The

616 calculated mean and standard deviation of the observation-based trend, however, does not take
617 into account the uncertainty associated with the observation-based estimates of $[\text{CO}_2]$,
618 consideration of which will increase the calculated standard deviation even more. The magnitudes
619 of trend in Φ_{CO_2} simulated by CanESM2 ($\gamma_d=0.25$) and CanESM4.2 (for $\gamma_d=0.25$) are
620 0.103 ± 0.05 and 0.153 ± 0.031 , respectively, and statistically not different from the trend in the
621 observation-based value of Φ_{CO_2} implying an increase of 0.27 ± 0.13 and 0.40 ± 0.08 ppm,
622 respectively, in Φ_{CO_2} over the 1980-2005 period. The statistical difference is calculated on the
623 basis of $\bar{x} \pm 1.385 \sigma_x$ range which corresponds to 83.4% confidence intervals; the estimates from
624 two sources are statistically not different at the 95% confidence level if this range overlaps (Knol
625 et al., 2011). The magnitudes of the trend in Φ_{CO_2} over the 1980-2005 period for CanESM4.2
626 simulations with $\gamma_d = 0.4$ and 0.55 (0.328 ± 0.038 and 0.314 ± 0.034 ppm/10-years, respectively)
627 are, however, more than twice, and statistically different from the observation-based estimate
628 (0.142 ± 0.08 ppm/10-years).

629
630 Overall, the CanESM4.2 simulation with $\gamma_d=0.25$ yields the amplitude of the globally-average
631 annual CO_2 cycle and its rate of increase over the 1980-2005 period that compares best with
632 observation-based estimates.

633 634 **4.3. Historical simulations without LUC**

635
636 Figure 10 and 11 show results from CanESM4.2 emissions-driven simulations for three different
637 strengths of the CO_2 fertilization effect that do not implement anthropogenic LUC over the
638 historical period and compare them to their corresponding simulations with LUC.

639

640 Figure 10a compares the simulated $[\text{CO}_2]$; as expected in the absence of anthropogenic LUC the
641 simulated $[\text{CO}_2]$ is lower since LUC emissions do not contribute to increase in $[\text{CO}_2]$. The
642 difference in $[\text{CO}_2]$ at the end of the simulation, in year 2005, between simulations with and
643 without LUC is 29.0, 23.6 and 19.0 ppm for $\gamma_d=0.25$, 0.40 and 0.55. The simulations with the
644 lowest strength of the CO_2 fertilization effect ($\gamma_d=0.25$) yield the largest difference because these
645 simulations also have the largest $[\text{CO}_2]$ amongst their set of simulations with and without LUC.
646 The CO_2 fertilization of the terrestrial biosphere implies that the effect of deforestation will be
647 higher, because of reduced carbon uptake by deforested vegetation, if background $[\text{CO}_2]$ is
648 higher.

649

650 Figure 10b compares the simulated NPP from CanESM4.2 simulations with and without LUC.
651 The increase in simulated NPP, regardless of the strength of the CO_2 fertilization effect, is lower
652 over the historical period in simulations without LUC for two apparent reasons. First, the rate of
653 increase of $[\text{CO}_2]$ is itself lower and second, in the absence of LUC, there is no contribution from
654 increasing crop area to NPP. Overall, the increase in NPP over the 1850-2005 period in
655 simulations with LUC is a little more than twice that in simulations without LUC. Figure 10c and
656 10d compare the changes in global vegetation biomass and soil carbon mass, over the historical
657 period, from simulations with and without LUC. As expected, in the absence of LUC, global
658 vegetation biomass and soil carbon mass more or less show a continuous increase, associated with
659 the increase in NPP which itself is due to the increase in $[\text{CO}_2]$. Consequently, in Figure 11a, the
660 cumulative atmosphere-land CO_2 flux \tilde{F}_L in simulations without LUC also shows a more or less
661 continuous increase over the historical period.

662

663 Finally, Figure 11b shows the diagnosed cumulative LUC emissions \tilde{E}_L calculated as the
664 difference between cumulative \tilde{F}_L , following equation 10, from simulations with and without
665 LUC. The diagnosed \tilde{E}_L in this manner are equal to 95, 81 and 67 Pg C, over the 1850-2005
666 period, for $\gamma_d=0.25$, 0.40 and 0.55. The calculated diagnosed \tilde{E}_L are highest for $\gamma_d=0.25$
667 associated with the highest background simulated $[\text{CO}_2]$ in these simulations, as mentioned
668 earlier. For comparison, LUC emissions estimated by Houghton (2008) for the period 1850-2005,
669 based on a book-keeping approach, are 156 Pg C but these estimates are generally believed to be
670 $\pm 50\%$ uncertain (see Figure 1 of Ramankutty et al. (2007)). LUC emissions, when calculated by
671 differencing F_L from simulations with and without LUC, also depend on the type of simulations
672 performed - in particular, if simulations are driven with specified CO_2 concentrations or specified
673 CO_2 emissions. Had our simulations been concentration-driven, in contrast to being emissions
674 driven, then both with and without LUC simulations would have experienced the same specified
675 observed CO_2 concentration over the historical period and the simulated LUC emissions would
676 have been higher. Arora and Boer (2010) found that diagnosed LUC emissions in the first version
677 of the Canadian Earth System Model (CanESM1) increased from 71 Pg C (for emissions-driven
678 simulations) to 124 Pg C (for concentration-driven simulations). Concentration-driven
679 simulations, however, cannot be evaluated against observation-based amplitude of the annual CO_2
680 cycle and its increase over the historical period. These simulations either ignore the annual cycle
681 of CO_2 (our specified- CO_2 case) or use a specified amplitude of the CO_2 annual cycle (our
682 relaxed- CO_2 case).

683

684 **5.0. Discussion and conclusions**

685
686
687
688
689
690
691
692
693
694
695
696
697
698
699
700
701
702
703
704
705
706
707

This study evaluates the ability of four observation-based determinants of the global carbon cycle and the historical carbon budget to constrain the parameterization of photosynthesis down-regulation, which directly determines the strength of the CO₂ fertilization effect, over the historical period 1850-2005. The key parameter that controls the strength of the CO₂ fertilization effect in CTEM, γ_d , was varied in the latest version of CCCma's earth system model CanESM4.2. Comparing simulated and observation-based estimates of 1) globally-averaged atmospheric CO₂ concentration, 2) cumulative atmosphere-land CO₂ flux, and 3) atmosphere-land CO₂ flux for the decades of 1960s, 1970s, 1980s, 1990s and 2000s, it is found that the CanESM4.2 version with $\gamma_d=0.40$ yields the best comparison.

The evaluation of CTEM within the framework of CanESM4.2 presented here is based on an emergent model property at the global scale and may be considered as a top-down approach of model evaluation. In contrast, the bottom-up approaches of model evaluation typically evaluate model results and processes against observations of primary atmosphere-land carbon and/or nitrogen fluxes and sizes of the vegetation, litter and soil carbon/nitrogen pools (e.g. Zaehle et al., 2014). Indeed, CTEM has been evaluated at point (e.g. Arora and Boer, 2005; Melton et al., 2015), regional (e.g. Peng et al., 2014; Garnaud et al., 2014) and global (e.g. Arora and Boer, 2010; Melton and Arora, 2014) scales in a number of studies when driven with observation-based reanalysis data. Both top-down and bottom-up approaches of model evaluation are complimentary to each other and allow to evaluate different aspects of the model at different spatial and temporal scales.

708 For the top-down approach used here, CanESM4.2 simulates globally-averaged near-surface
709 [CO₂] of 400, **381** and 368 ppm for $\gamma_d=0.25$, **0.40** and 0.55, respectively, compared to the
710 observation-based estimate of **379** ppm for year 2005. The cumulative atmosphere-land CO₂ flux
711 of 18 Pg C for the period 1850-2005 for $\gamma_d=0.40$ lies within the range of the observation-based
712 estimate of -11 ± 47 Pg C in Figure 4b, and so do the average atmosphere-land CO₂ flux for the
713 decades of 1960s through to 2000s in Figure 4a when compared to observation-based estimates
714 from Le Quéré et al. (2015). $\gamma_d=0.25$ and 0.55 yield average atmosphere-land CO₂ flux for the
715 decades of 1960s through to 2000s that are lower and higher, respectively, than the observation-
716 based estimates from Le Quéré et al. (2015). The only determinant against which $\gamma_d=0.40$ does
717 not yield the best comparison with observation-based estimates is the amplitude of the globally-
718 averaged annual CO₂ cycle and its increase over the 1980 to 2005 period. For this determinant,
719 $\gamma_d=0.25$ seems to yield the best comparison (Figure 9). The value of $\gamma_d=0.40$ that yields best
720 overall comparison with observation-based determinants of the global carbon cycle and the
721 historical carbon budget is also broadly consistent with Arora et al. (2009) who derived a value of
722 $\gamma_d=0.46$ based on results from FACE studies (as mentioned in Section 2.2.2).

723

724 The caveat with the analyses presented here, or for any model for that matter, is that the strength
725 of the terrestrial CO₂ fertilization effect is dependent on the processes included in the model and
726 the parameter values associated with them. The primary example of this is the adjustment to the
727 humification factor in CTEM4.2, which leads to reduction in the global soil carbon amount as
728 anthropogenic LUC becomes significant towards the mid-20th Century. This response of soil
729 carbon was not present in the model's configuration of CTEM and historical simulations made
730 with CanESM2. The representation of soil carbon loss, in response to anthropogenic LUC in

731 CanESM4.2, implies that a stronger CO₂ fertilization effect (or weaker photosynthesis down-
732 regulation) should be required to reproduce realistic atmosphere-land CO₂ flux over the historical
733 period and this was found to be the case in Figure 4a. Despite this dependence on processes
734 included in the model, the response of the land carbon cycle, over the historical period, to the two
735 primary forcings of increased [CO₂] and anthropogenic land use change must be sufficiently
736 realistic in the model to satisfy all the four determinants of the global carbon cycle and the
737 historical global carbon budget.

738

739 The simulated loss in soil carbon in response to anthropogenic LUC over the historical period
740 may also be assessed against observation-based estimates from Wei et al. (2014). Using data from
741 453 sites that were converted from forest to agricultural land, Wei et al. (2014) find that the soil
742 organic carbon stocks decreased by an average of $43.1 \pm 1.1\%$ for all sites. Based on the HYDE
743 v3.1 data set from which the changes in crop area are derived (Hurtt et al., 2011), LUC as
744 implemented in CanESM4.2 yields an increase in crop area from about 5 million km² in 1850 to
745 about 15 million km² in 2005. Assuming an initial soil carbon amount of 10 Kg C/m² (see Figure
746 2c of Melton and Arora (2014)) and an average 40% decrease in soil carbon amount, based on
747 Wei et al. (2014), implies that the increase in crop area of about 10 million km² over the historical
748 period has likely yielded a global soil organic carbon loss of 40 Pg C. The loss in soil carbon in
749 Figure 5a is simulated to 18 Pg C for CanESM4.2 simulation with $\gamma_d = 0.40$, the simulation that
750 yield best comparison with observation-based determinants of the global carbon cycle and the
751 historical carbon budget. This loss of 18 Pg C is expected to be less than the 40 Pg C because the
752 model estimates also include an increase associated with the increase in NPP due to the CO₂
753 fertilization effect from non-crop areas. The effect of LUC on global soil carbon loss may also by

754 estimated by differencing global soil carbon amounts from simulations with and without LUC
755 from Figure 10d at the end of the simulation in year 2005. For CanESM4.2 simulation with $\gamma_d =$
756 0.40, this amounts to around 50 Pg C. Both these estimates of soil carbon loss are broadly
757 consistent with the back-of-the-envelope calculation of 40 Pg C soil carbon loss, based on Wei et
758 al. (2014) estimates, indicating that the soil carbon loss simulated in response to anthropogenic
759 LUC over the historical period is not grossly over or underestimated.

760

761 The CanESM4.2 simulation with $\gamma_d = 0.40$, however, fails to satisfy the rate of increase of the
762 amplitude of the globally-averaged annual CO₂ cycle over the 1980-2005 period implying that
763 there are still limitations in the model structure and/or parameter values. Of course, the fact that
764 the amplitude of the globally-averaged annual CO₂ cycle is also affected by the atmosphere-ocean
765 CO₂ fluxes makes it more difficult to attribute the changes in the amplitude of the globally-
766 averaged annual CO₂ cycle solely to atmosphere-land CO₂ fluxes. Additionally, the increase in
767 crop area as well as crop yield per unit area over the historical period have been suggested by
768 Zeng et al. (2014) to contribute towards the observed increase in the amplitude of annual CO₂
769 cycle. Based on their sensitivity tests, Zeng et al. (2014) attribute 45, 29 and 26 percent of the
770 observed increase in the seasonal-cycle amplitude of the CO₂ cycle to LUC, climate variability
771 and change (including factors such as the lengthening of the growing season) and increased
772 productivity due to CO₂ fertilization, respectively. Comparison of the rate of increase of NPP in
773 CanESM4.2 experiments with and without LUC (Figure 10b), as a measure of increase in the
774 strength of the CO₂ fertilization effect, suggests that the contribution of anthropogenic LUC to the
775 increase in the seasonal-cycle amplitude is 52%, which is broadly consistent with the 45% value
776 obtained by Zeng et al. (2014).

777

778 While CanESM4.2 simulation with $\gamma_d=0.40$ is able to simulate a realistic rate of increase of
779 $[\text{CO}_2]$ over the period 1960 to 2005, the modelled atmosphere-ocean CO_2 fluxes for this and the
780 CanESM2 version are lower than observational estimates of this quantity (Figure 8). This implies
781 that if the modelled atmosphere-ocean CO_2 flux were to increase and become more consistent
782 with observation-based estimates then the modelled atmosphere-land CO_2 flux must decrease to
783 still be able to yield sufficiently realistic rate of increase of $[\text{CO}_2]$. This implies that the strength
784 of the terrestrial CO_2 fertilization effect should likely be somewhat lower than what is obtained by
785 $\gamma_d=0.40$ or the simulated atmosphere-land CO_2 flux is higher because of some other reason, most
786 likely lower LUC emissions. Indeed, the required decrease in modelled atmosphere-land CO_2 flux
787 is consistent with the fact that the modelled LUC emissions for $\gamma_d=0.40$ (81 Pg C) are about half
788 the estimate from Houghton (2008) (156 Pg C) with the caveat, of course, that Houghton's
789 estimates themselves have an uncertainty of roughly $\pm 50\%$. The LUC module of CTEM currently
790 only accounts for changes in crop area and does not take into account changes associated with
791 pasture area given their ambiguous definition (pasture may or may not be grasslands). The model
792 also does not take into account wood harvesting which amongst other uses is also used as a
793 biofuel. Treatment of these additional processes will increase modelled LUC emissions.

794

795 Although the CanESM4.2 simulation with $\gamma_d=0.40$ satisfies three out of four constraints placed
796 by the chosen determinants of the global carbon cycle and the historical carbon budget, and also
797 simulates reasonable soil carbon loss in response to anthropogenic LUC, the model now yields
798 the highest land carbon uptake, in the 1pctCO2 experiment, amongst the CMIP5 models that were
799 compared by Arora et al. (2013) as seen in Figure 2. Of course, the 1pctCO2 experiment is in no

800 way indicative of models' performance over the historical period, nor is being an outlier amongst
801 CMIP5 models a conclusive evaluation of CanESM4.2's land carbon uptake. However, it remains
802 possible that the chosen determinants of the global carbon cycle and the historical carbon budget
803 are not able to constrain the model sufficiently, given the especially large uncertainty associated
804 with LUC emissions. Nevertheless, these observation-based constraints of the carbon cycle and
805 historical carbon budget are essentially the only means to evaluate carbon cycle aspects of the
806 ESMs at the global scale including the strength of the terrestrial CO₂ fertilization effect. In the
807 near future, availability of model output from the sixth phase of CMIP (CMIP6) will allow a
808 comparison of the simulated aspects of the global carbon cycle and the historical carbon budget
809 from ESMs to observations-based estimates for the 1850-2014 period. These data will allow a
810 comparison of the rate of increase of the amplitude of globally-averaged surface [CO₂] in models
811 with observation-based estimates over a longer period. This should help better constrain the
812 strength of the terrestrial CO₂ fertilization effect, as it is represented in models, in a somewhat
813 more robust manner.

814

815 **6.0 Source code and data availability**

816 Source code for the complete CanESM4.2 model is an extremely complex set of FORTRAN
817 subroutines, with C preprocessor (CPP) directives, that reside in CCCma libraries. Unix shell
818 scripts process the model code for compilation based on CPP directives and several other
819 switches (e.g. those related to free-CO₂, specified-CO₂, and relaxed-CO₂ settings). As such, it is
820 extremely difficult to make the full model code available. However, selected model subroutines
821 related to specific physical and biogeochemical processes can be made available by either author
822 (vivek.arora@canada.ca, john.scinocca@canada.ca) upon agreeing to Environment and Climate

823 Change Canada's software licensing agreement available at
824 <http://collaboration.cmc.ec.gc.ca/science/rpn.comm/license.html>. Data used to produce plots and
825 figures can be obtained from the first author (vivek.arora@canada.ca).

826

827 **Copyright statement**

828 The works published in this journal are distributed under the Creative Commons Attribution 3.0
829 License. This license does not affect this Crown copyright work, which is re-usable under the
830 Open Government License (OGL). The Creative Commons Attribution 3.0 License and the OGL
831 are interoperable and do not conflict with, reduce or limit each other. ©Crown copyright 2015.

832

833 **Acknowledgements**

834 We would like to thank Joe Melton and Neil Swart for providing comments on an earlier version
835 of this paper. We also thank the three anonymous reviewers for their constructive and helpful
836 comments.

837

838 **References**

- 839 Arora, V. K. and Boer, G. J. (2005) A parameterization of leaf phenology for the terrestrial ecosystem
840 component of climate models, *Glob. Change Biol.*, 11, 39–59, doi:10.1111/j.1365-
841 2486.2004.00890.x.
- 842 Arora, V. K. and Boer, G. J. (2014) Terrestrial ecosystems response to future changes in climate and
843 atmospheric CO₂ concentration, *Biogeosciences*, 11, 4157-4171, doi:10.5194/bg-11-
844 4157-2014 Arora, V. K. and Boer, G. J. (2014) Terrestrial ecosystems response to future
845 changes in climate and atmospheric CO₂ concentration, *Biogeosciences Discuss.*, 11,
846 3581-3614, doi:10.5194/bgd-11-3581-2014.
- 847 Arora, V. K., G. J. Boer, J. R. Christian, C. L. Curry, K. L. Denman, K. Zahariev, G. M. Flato, J. F.
848 Scinocca, W. J. Merryfield, and W. G. Lee (2009) The effect of terrestrial photosynthesis
849 down-regulation on the 20th century carbon budget simulated with the CCCma Earth
850 System Model, *J. Clim.*, 22, 6066-6088.
- 851 Arora, V. K., G. J. Boer, P. Friedlingstein, M. Eby, C. D. Jones, J. R. Christian, G. Bonan, L. Bopp,
852 V. Brovkin, P. Cadule, T. Hajima, T. Ilyina, K. Lindsay, J. F. Tjiputra, T. Wu (2013)
853 Carbon-Concentration and Carbon-Climate Feedbacks in CMIP5 Earth System Models.
854 *Journal of Climate*, Vol. 26, Iss. 15, pp. 5289-5314.
- 855 Arora, V. K., J. F. Scinocca, G. J. Boer, J. R. Christian, K. L. Denman, G. M. Flato, V. V. Kharin, W.
856 G. Lee, and W. J. Merryfield (2011) Carbon emission limits required to satisfy future
857 representative concentration pathways of greenhouse gases, *Geophys. Res. Lett.*, 38,
858 L05805, doi:10.1029/2010GL046270.
- 859 Arora, V.K. and G.J. Boer (2010) Uncertainties in the 20th century carbon budget associated with
860 land use change, *Global Change Biology*, 16(12), 3327-3348.
- 861 Bartlett, P. A., Mackay, M. D., and Verseghy, D. L. (2006) Modified snow algorithms in the Canadian
862 Land Surface Scheme: model runs and sensitivity analysis at three boreal forest stands,
863 *Atmos. Ocean*, 44, 207–222.
- 864 Bartlett, P. and Verseghy, D. (2015) Modified treatment of intercepted snow improves the
865 simulated forest albedo in the Canadian Land Surface Scheme, *Hydrol. Process.*, 29, 3208–
866 3226, doi:10.1002/hyp.10431.
- 867 Brown, R., Bartlett, P., Mackay, M., and Verseghy, D. (2006) Estimation of snow cover in CLASS for
868 SnowMIP, *Atmos. Ocean*, 44, 223–238.

869 Christian, J. R., and coauthors (2010) The global carbon cycle in the Canadian Earth system model
870 (CanESM1): Preindustrial control simulation, *J. Geophys. Res.*, 115, G03014,
871 doi:10.1029/2008JG000920.

872 Ciais, P., C. Sabine, G. Bala, L. Bopp, V. Brovkin, J. Canadell, A. Chhabra, R. DeFries, J. Galloway,
873 M. Heimann, C. Jones, C. Le Quéré, R.B. Myneni, S. Piao and P. Thornton (2013) Carbon
874 and Other Biogeochemical Cycles. In: *Climate Change 2013: The Physical Science Basis*.
875 Contribution of Working Group I to the Fifth Assessment Report of the Intergovernmental
876 Panel on Climate Change [Stocker, T.F., D. Qin, G.-K. Plattner, M. Tignor, S.K. Allen, J.
877 Boschung, A. Nauels, Y. Xia, V. Bex and P.M. Midgley (eds.)]. Cambridge University
878 Press, Cambridge, United Kingdom and New York, NY, USA.

879 da Rocha, H.R., M.L. Goulden, S.D. Miller, M.C. Menton, L.D.V.O. Pinto, H.C. De Freitas, and
880 A.M.E. Silva Figueira (2004): Seasonality of water and heat fluxes over a tropical forest
881 in eastern Amazonia, *Ecological Applications*, 14(4) Supplement, S22-S32.

882 Friedlingstein, P., P. Cox, R. Betts, L. Bopp, W. von Bloh, V. Brovkin, P. Cadule, S. Doney, M. Eby,
883 I. Fung, G. Bala, J. John, C. Jones, F. Joos, T. Kato, M. Kawamiya, W. Knorr, K. Lindsay,
884 H. D. Matthews, T. Raddatz, P. Rayner, C. Reick, E. Roeckner, K.-G. Schnitzler, R.
885 Schnur, K. Strassmann, A. J. Weaver, C. Yoshikawa, N. Zeng. 2006: Climate–carbon
886 cycle feedback analysis: Results from the C4MIP model intercomparison, *J. Clim.*, 19(14),
887 3337-3353.

888 G. C. Hurtt, L. P. Chini, S. Froking, R. A. Betts, J. Feddema, G. Fischer, J. P. Fisk, K. Hibbard, R. A.
889 Houghton, A. Janetos, C. D. Jones, G. Kindermann, T. Kinoshita, Kees Klein Goldewijk,
890 K. Riahi, E. Shevliakova, S. Smith, E. Stehfest, A. Thomson, P. Thornton, D. P. van
891 Vuuren, Y. P. Wang (2011) Harmonization of land-use scenarios for the period 1500-
892 2100: 600 years of global gridded annual land-use transitions, wood harvest, and resulting
893 secondary lands. *Climatic Change*, 109, 117-161, doi:10.1007/s10584-011-0153-2.

894 Garnaud, C., L. Sushama, V. K. Arora (2014) The effect of driving climate data on the simulated
895 terrestrial carbon pools and fluxes over North America, *International Journal of*
896 *Climatology* 34 (4), 1098-1110.

897 Gillett, N. P., V. K. Arora, D. Matthews, M. R. Allen (2013) Constraining the Ratio of Global
898 Warming to Cumulative CO₂ Emissions Using CMIP5 Simulations. *Journal of Climate*,
899 Vol. 26, Iss. 18, pp. 6844-6858.

900 Gourджи, S. M., K. L. Mueller, V. Yadav, D. N. Huntzinger, A. E. Andrews, M. Trudeau, G. Petron, T.
901 Nehr Korn, J. Eluszkiewicz, J. Henderson, D. Wen, J. Lin, M. Fischer, C. Sweeney, and A.
902 M. Michalak (2012) North American CO₂ exchange: inter-comparison of modeled
903 estimates with results from a fine-scale atmospheric inversion, *Biogeosciences*, 9, 457–
904 475, doi:10.5194/bg-9-457-2012.

905 Hoffman, F. M., J. T. Randerson, V. K. Arora, Q. Bao, P. Cadule, D. Ji, C. D. Jones, M. Kawamiya,
906 S. Khatiwala, K. Lindsay, A. Obata, E. Shevliakova, K. D. Six, J. F. Tjiputra, E. M.
907 Volodin, and T. Wu (2014) Causes and implications of persistent atmospheric
908 carbondioxide biases in Earth System Models, *J. Geophys. Res. Biogeosci.*, 119, 141–162,
909 doi:10.1002/2013JG002381.

910 Houghton, R.A. 2008. Carbon Flux to the Atmosphere from Land-Use Changes: 1850-2005. In
911 *TRENDS: A Compendium of Data on Global Change*. Carbon Dioxide Information
912 Analysis Center, Oak Ridge National Laboratory, U.S. Department of Energy, Oak Ridge,
913 Tenn., U.S.A.

914 Jones, C., E. Robertson, V. Arora, P. Friedlingstein, E. Shevliakova, L. Bopp, V. Brovkin, T. Hajima,
915 E. Kato, M. Kawamiya, S. Liddicoat, K. Lindsay, C.H. Reick, C. Roelandt, J.
916 Segschneider, J. Tjiputra (2013) Twenty-First-Century Compatible CO₂ Emissions and
917 Airborne Fraction Simulated by CMIP5 Earth System Models under Four Representative
918 Concentration Pathways. *Journal of Climate*, Vol. 26, Iss. 13, pp. 4398-4413.

919 Keeling, C. D., Chin, J. F. S. & Whorf, T. P. (1996) Increased activity of northern vegetation inferred
920 from atmospheric CO₂ measurements. *Nature* 382, 146–149.

921 Khatiwala, S., F. Primeau, and T. Hall (2009) Reconstruction of the history of anthropogenic CO₂
922 concentrations in the ocean. *Nature*, 462, 346–349.

923 Knol, M. J., W. R. Pestman, and D. E. Grobbee (2011) The (mis)use of overlap of confidence
924 intervals to assess effect modification, *Eur. J. Epidemiol.*, 26(4), 253–254.

925 Knorr, W. (2009) Is the airborne fraction of anthropogenic CO₂ emissions increasing?, *Geophys. Res.*
926 *Lett.*, 36, L21710, doi:10.1029/2009GL040613.

927 Le Quéré, C., Moriarty, R., Andrew, R. M., Peters, G. P., Ciais, P., Friedlingstein, P., Jones, S. D.,
928 Sitch, S., Tans, P., Arneeth, A., Boden, T. A., Bopp, L., Bozec, Y., Canadell, J. G., Chini,
929 L. P., Chevallier, F., Cosca, C. E., Harris, I., Hoppema, M., Houghton, R. A., House, J. I.,
930 Jain, A. K., Johannessen, T., Kato, E., Keeling, R. F., Kitidis, V., Klein Goldewijk, K.,
931 Koven, C., Landa, C. S., Landschützer, P., Lenton, A., Lima, I. D., Marland, G., Mathis, J.

932 T., Metzl, N., Nojiri, Y., Olsen, A., Ono, T., Peng, S., Peters, W., Pfeil, B., Poulter, B.,
933 Raupach, M. R., Regnier, P., Rödenbeck, C., Saito, S., Salisbury, J. E., Schuster, U.,
934 Schwinger, J., Séférian, R., Segschneider, J., Steinhoff, T., Stocker, B. D., Sutton, A. J.,
935 Takahashi, T., Tilbrook, B., van der Werf, G. R., Viovy, N., Wang, Y.-P., Wanninkhof,
936 R., Wiltshire, A., and Zeng, N. (2015) Global carbon budget 2014, *Earth Syst. Sci. Data*,
937 7, 47-85, doi:10.5194/essd-7-47-2015.

938 Ma, X., von Salzen, K., and Li, J. (2008) Modelling sea salt aerosol and its direct and indirect effects
939 on climate, *Atmos. Chem. Phys.*, 8, 1311–1327, doi:10.5194/acp-8-1311-2008.

940 McGuire, A. D., J. M. Melilli, and L. A. Joyce (1995): The role of nitrogen in the response of forest
941 net primary productivity to elevated atmospheric carbon dioxide, *Annual Reviews of*
942 *Ecology and Systematics*, 26, 473-503.

943 Medlyn, B. E., F. -W. Badeck, D. G. G. De Pury, C. V. M. Barton, M. Broadmeadow, R. Ceulemans,
944 P. De Angelis, M. Forstreuter, M. E. Jach, S. Kellomäki, E. Laitat, M. Marek, S. Philippot,
945 A. Rey, J. Strassmeyer, K. Laitinen, R. Liozon, B. Portier, P. Roberntz, K. Wang, P. G.
946 Jstbid (1999): Effects of elevated [CO₂] on photosynthesis in European forest species: a
947 meta-analysis of model parameters, *Plant, Cell & Environment*, 22, 1475–1495.

948 Melton, J. R. and Arora, V. K. (2014) Sub-grid scale representation of vegetation in global land
949 surface schemes: implications for estimation of the terrestrial carbon sink, *Biogeosciences*,
950 11, 1021-1036, doi:10.5194/bg-11-1021-2014.

951 Melton, J. R. and Arora, V. K. (2014) Sub-grid scale representation of vegetation in global land
952 surface schemes: implications for estimation of the terrestrial carbon sink, *Biogeosciences*,
953 11, 1021-1036, doi:10.5194/bg-11-1021-2014.

954 Melton, J. R., Shrestha, R. K., and Arora, V. K. (2015) The influence of soils on heterotrophic
955 respiration exerts a strong control on net ecosystem productivity in seasonally dry
956 Amazonian forests, *Biogeosciences*, 12, 1151-1168, doi:10.5194/bg-12-1151-2015.

957 Namazi, M., von Salzen, K., and Cole, J. N. S. (2015) Simulation of black carbon in snow and its
958 climate impact in the Canadian Global Climate Model, *Atmos. Chem. Phys. Discuss.*, 15,
959 18839-18882, doi:10.5194/acpd-15-18839-2015.

960 Peng, Y., Arora, V. K., Kurz, W. A., Hember, R. A., Hawkins, B. J., Fyfe, J. C., and Werner, A. T.
961 (2014) Climate and atmospheric drivers of historical terrestrial carbon uptake in the
962 province of British Columbia, Canada, *Biogeosciences*, 11, 635-649, doi:10.5194/bg-11-
963 635-2014.

964 Peng, Y., von Salzen, K., and Li, J. (2012) Simulation of mineral dust aerosol with Piecewise Log-
965 normal Approximation (PLA) in CanAM4-PAM, *Atmos. Chem. Phys.*, 12, 6891–6914, 30
966 doi:10.5194/acp-12-6891-2012.

967 Phillips, O. L. and S. L. Lewis (2014) Evaluating the tropical forest carbon sink, *Global Change*
968 *Biology* (2014) 20, 2039–2041, doi: 10.1111/gcb.12423.

969 Pongratz, J., Reick, C. H., Houghton, R. A., and House, J. I. (2014) Terminology as a key uncertainty
970 in net land use and land cover change carbon flux estimates, *Earth Syst. Dynam.*, 5, 177-
971 195, doi:10.5194/esd-5-177-2014.

972 Ramankutty, N., H. K. Gibbs, F. Archard, R. DeFries, J. A. Foley, and R. A. Houghton (2007):
973 Challenges to estimating carbon emissions from tropical deforestation , *Global Change*
974 *Biology*, 13(1), 51-66.

975 Randerson, J. T., Thompson, M. V., Conway, T. J., Fung, I. Y. & Field, C. B. (1997) The contribution
976 of terrestrial sources and sinks to trends in the seasonal cycle of atmospheric carbon
977 dioxide. *Glob. Biogeochem. Cycles* 11, 535–560.

978 Schimel, D., Stephens, B. B., and Fisher, J. B.: Effect of increasing CO₂ on the terrestrial carbon
979 cycle (2015) *Proceedings of the National Academy of Science U.S.A.*, 112, 436–441,
980 doi:10.1073/pnas.1407302112, 2015.

981 Sturm, M., Holmgren, J., König, M., and Morris, K. (1997) The thermal conductivity of seasonal
982 snow, *J. Glaciol.*, 43, 26–41.

983 Tabler, R. D., Benson, C. S., Santana, B. W., and Ganguly, P. (1990) Estimating snow transport from
984 30 wind speed records: estimates versus measurements at Prudhoe Bay, Alaska, in: *Proc.*
985 *58th Western Snow Conf.*, Sacramento, CA, 61–78.

986 Taylor, Karl E., Ronald J. Stouffer, Gerald A. Meehl, 2012: An Overview of CMIP5 and the
987 Experiment Design. *Bull. Amer. Meteor. Soc.*, 93, 485–498.

988 Verseghy, D. L. (2012) CLASS-the Canadian land surface scheme (version 3.6)—technical
989 documentation. Internal report, Climate Research Division, Science and Technology
990 Branch, Environment Canada (Downsview, Toronto, Ontario)

991 von Salzen, K. (2006) Piecewise log-normal approximation of size distributions for aerosol
992 modelling, *Atmos. Chem. Phys.*, 6, 1351–1372, doi:10.5194/acp-6-1351-2006.

993 von Salzen, K., and Coauthors, 2013: The Canadian fourth generation atmospheric global climate
994 model (CanAM4). Part I: Representation of physical processes. *Atmos. Ocean*, 51,
995 doi:10.1080/07055900.2012.75561.

996 Wei, X., M. Shao, W. Gale and L. Li (2014) Global pattern of soil carbon losses due to the conversion
997 of forests to agricultural land, *Scientific Reports* 4, Article number: 4062 (2014)
998 doi:10.1038/srep04062.

999 Zaehle, S., Medlyn, B. E., De Kauwe, M. G., Walker, A. P., Dietze, M. C., Hickler, T., Luo, Y.,
1000 Wang, Y.-P., El-Masri, B., Thornton, P., Jain, A., Wang, S., Warlind, D., Weng, E.,
1001 Parton, W., Iversen, C. M., Gallet-Budynek, A., McCarthy, H., Finzi, A., Hanson, P. J.,
1002 Prentice, I. C., Oren, R., and Norby, R. (2014) Evaluation of 11 terrestrial carbon–nitrogen
1003 cycle models against observations from two temperate Free-Air CO₂ Enrichment studies,
1004 *New Phytologist*, 202, 803–822, doi:10.1111/nph.12697.

1005 Zeng, N., Zhao, F., Collatz, G. J., Kalnay, E., Salawitch, R. J., West, T. O., Guanter, L. (2014) .
1006 Agricultural Green Revolution as a driver of increasing atmospheric CO₂ seasonal
1007 amplitude, *Nature*, 515(7527), 394-397.

1008 Zobler, L. 1986. A World Soil File for Global Climate Modelling. NASA Technical Memorandum
1009 87802. NASA Goddard Institute for Space Studies, New York, New York, U.S.A.
1010

1011

1012 Table 1: Summary of simulations performed for this study and the forcings used.

Simulation	1pctCO2	esmhistorical	esmhistorical_noluc
Simulation details	1% per year increasing CO ₂ simulation	1850-2005 historical simulation based on CMIP5 protocol	1850-2005 historical simulation based on CMIP5 protocol, but with no anthropogenic land use change
Purpose	To allow comparison of CanESM4.2 with CMIP5 models especially in terms of its land carbon uptake	To compare simulated aspects of the global carbon cycle and historical carbon budget with observation-based estimates	To diagnose LUC emissions by differencing atmosphere-land CO ₂ flux between historical simulations with and without LUC.
Length	140 years	156 years	
CO ₂ forcing	285 ppm at the start of the simulation and 1140 ppm after 140 years.	Historical CO ₂ forcing	
Land cover forcing	Land cover corresponds to its 1850 state	Land cover evolution is based on increase in crop area over the historical period	Land cover corresponds to its 1850 state
Non-CO ₂ greenhouse gases forcing	Concentration of non-CO ₂ GHGs is specified at their 1850 levels.	Concentration of non-CO ₂ GHGs is specified and evolves over the historical period based on the CMIP5 protocol	
Aerosols forcing	Emissions of aerosols and their precursors are specified at their 1850 levels.	Emissions of aerosols and their precursors are specified and evolve over the historical period based on the CMIP5 protocol	

1013

1014

1015

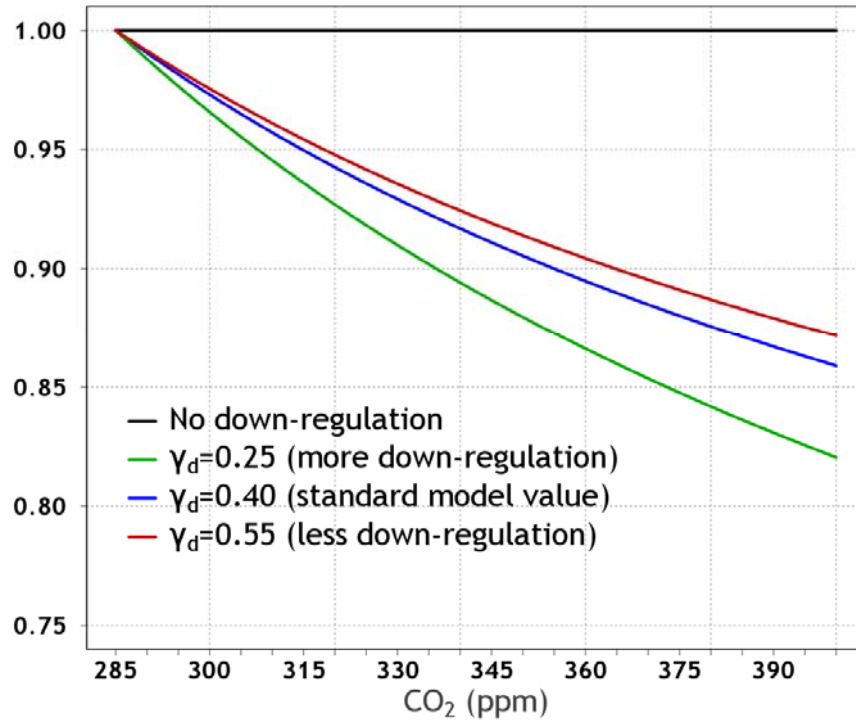
1016

1017

1018

1019

Down-regulation factor as a function of CO₂ concentration



1020

1021 Figure 1: The behaviour of terrestrial photosynthesis down-regulation scalar $\xi(C)$ (equation 12)
1022 for $\gamma_p=0.95$ and values of γ_d equal to 0.25, 0.4 and 0.55 that are used in CanESM4.2 simulations.

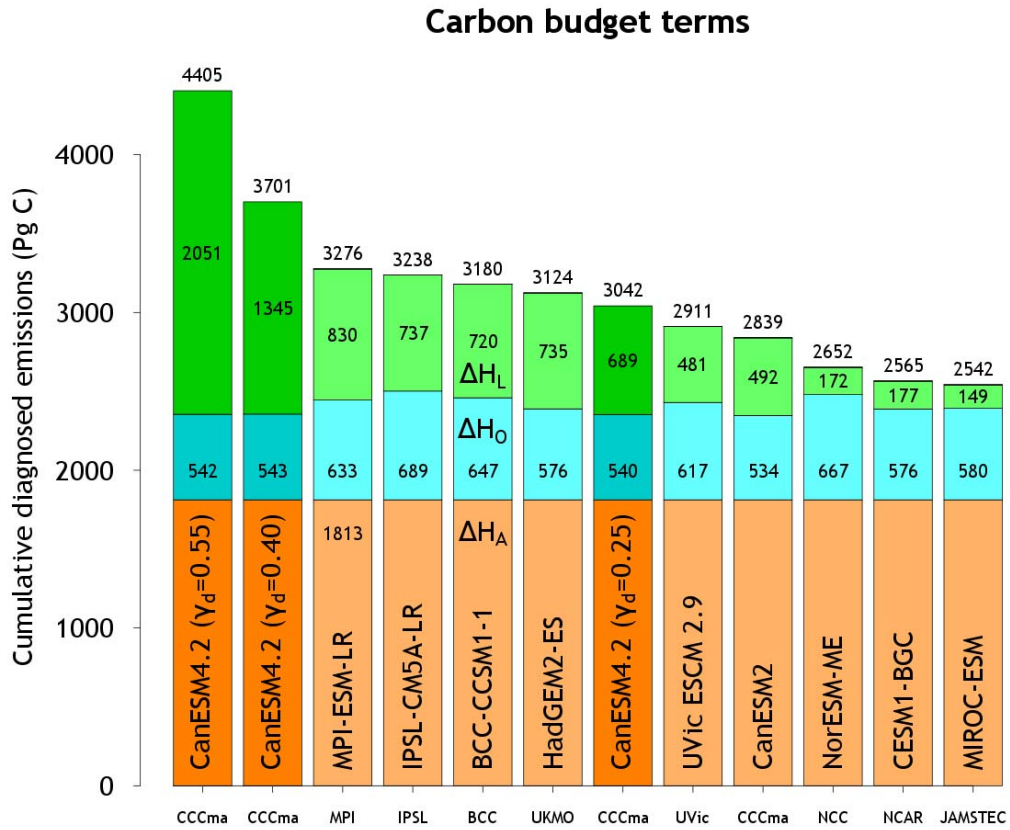
1023

1024

1025

1026

1027



1028

1029

1030

1031

1032

1033

1034

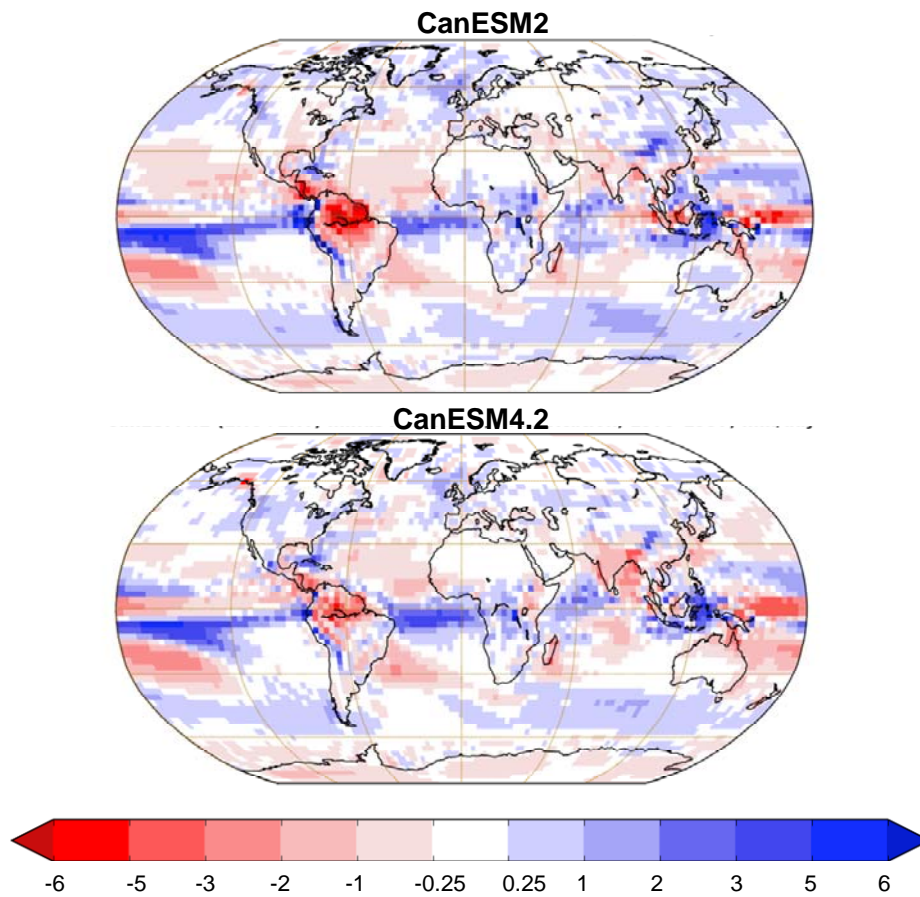
1035

Figure 2: Components of the carbon budget equation (8) that make up cumulative diagnosed emissions based on results from the fully-coupled 1pctCO₂ experiment. Results shown are from eight CMIP5 models that participated in the Arora et al. (2013) study and from three CanESM4.2 simulations (shown in darker colours) for three different strengths of the terrestrial CO₂ fertilization effect.

1036

1037

Model minus Xie and Arkin precipitation
averaged over the 1979-1998 period (mm/day)



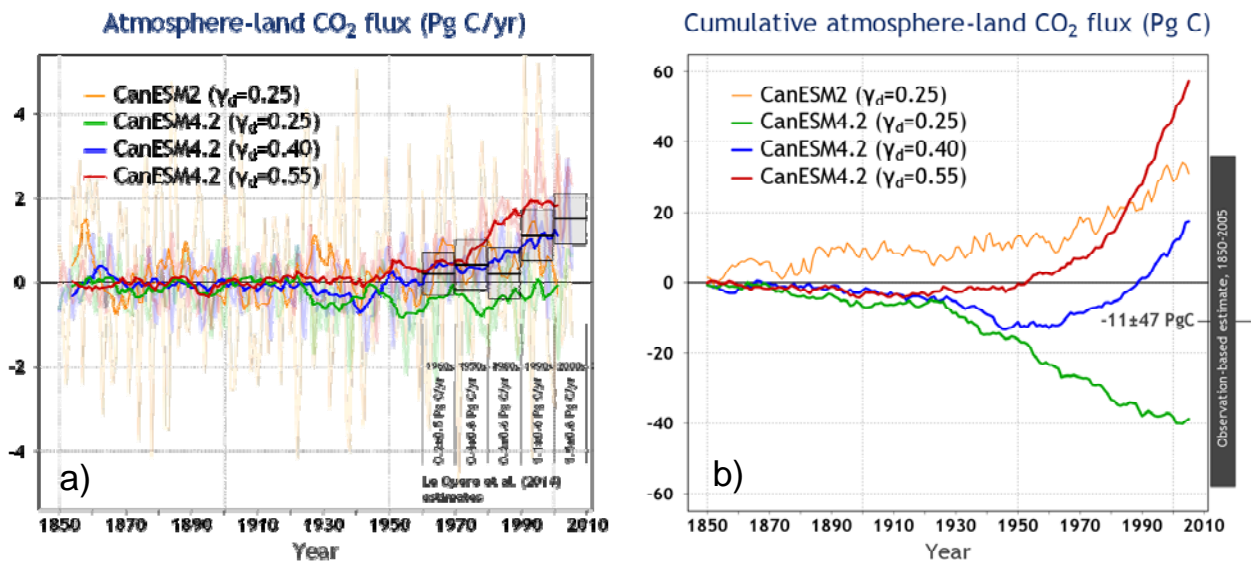
1038

1039

1040 Figure 3: CanESM2 (panel a) and CanESM4.2 (panel b, $\gamma_d=0.40$) precipitation anomalies
1041 compared to the observation-based estimates from CPC Merged Analysis of Precipitation
1042 (CMAP) based on Xie and Arkin (1997) averaged over the 1979–1998 period.

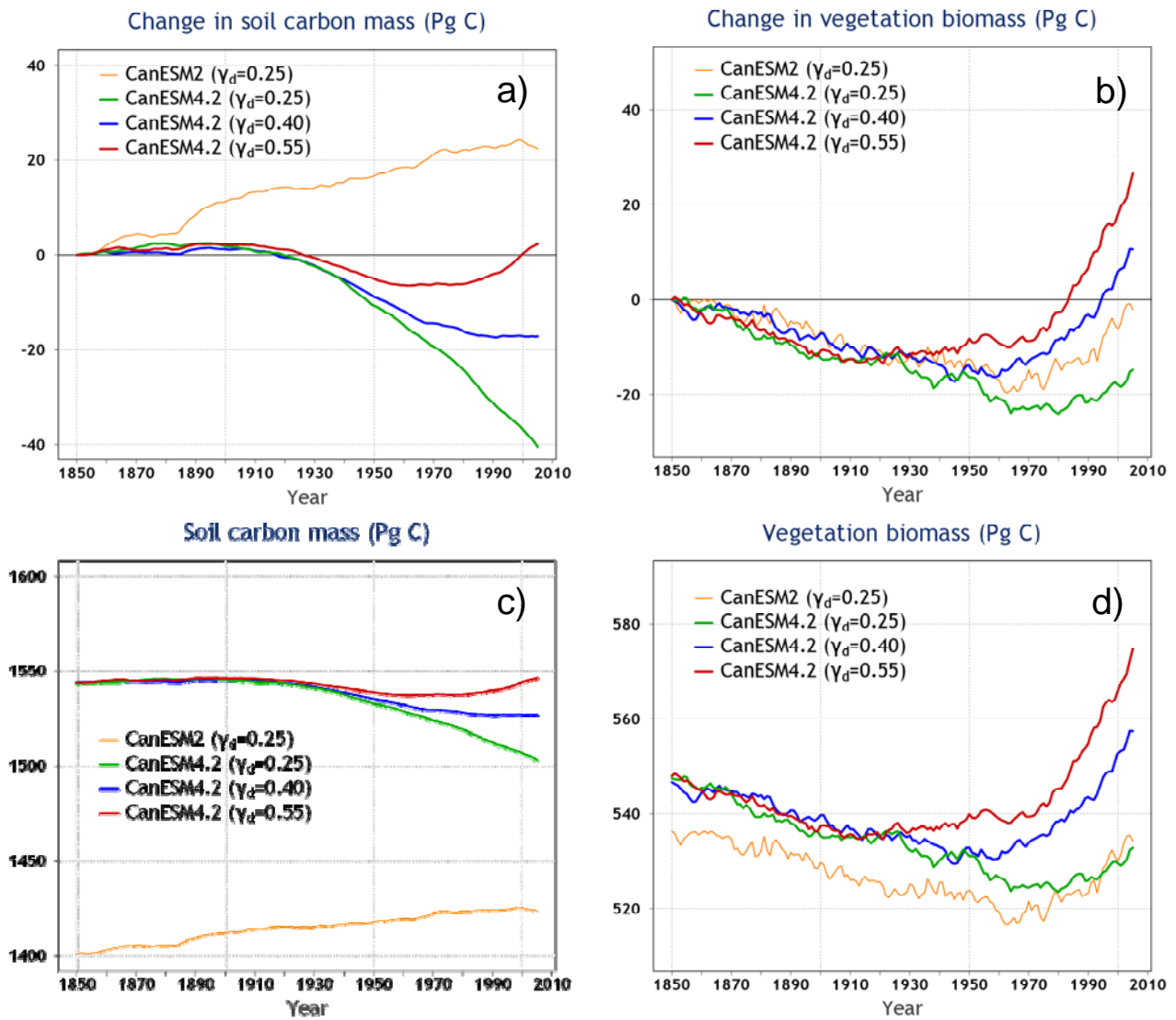
1043

1044
1045
1046
1047
1048



1049
1050
1051
1052
1053
1054
1055
1056
1057
1058

Figure 4: Atmosphere-land CO₂ flux (F_L) (panel a) and its cumulative values \tilde{F}_L (panel b) from CanESM2 and the three CanESM4.2 historical 1850-2005 simulations for different strengths of the terrestrial CO₂ fertilization effect. In panel (a) the observation-based estimates of F_L and their uncertainty, show via boxes, for the decades of 1960, 1970, 1980, 1990 and 2000 are reproduced from Le Quéré et al. (2015). The bold lines in panel (a) are the 10-year moving averages of the annual F_L values which are shown in light colours. The results from CanESM2 and CanESM4.2 are the average of the two ensemble members.



1060

1061 Figure 5: Change in and absolute values of global soil carbon and vegetation biomass amounts
 1062 from CanESM2 and the three CanESM4.2 historical 1850-2005 simulations with different
 1063 strengths of the terrestrial CO₂ fertilization effect. The results shown in all panels are the average
 1064 of the two ensemble members.

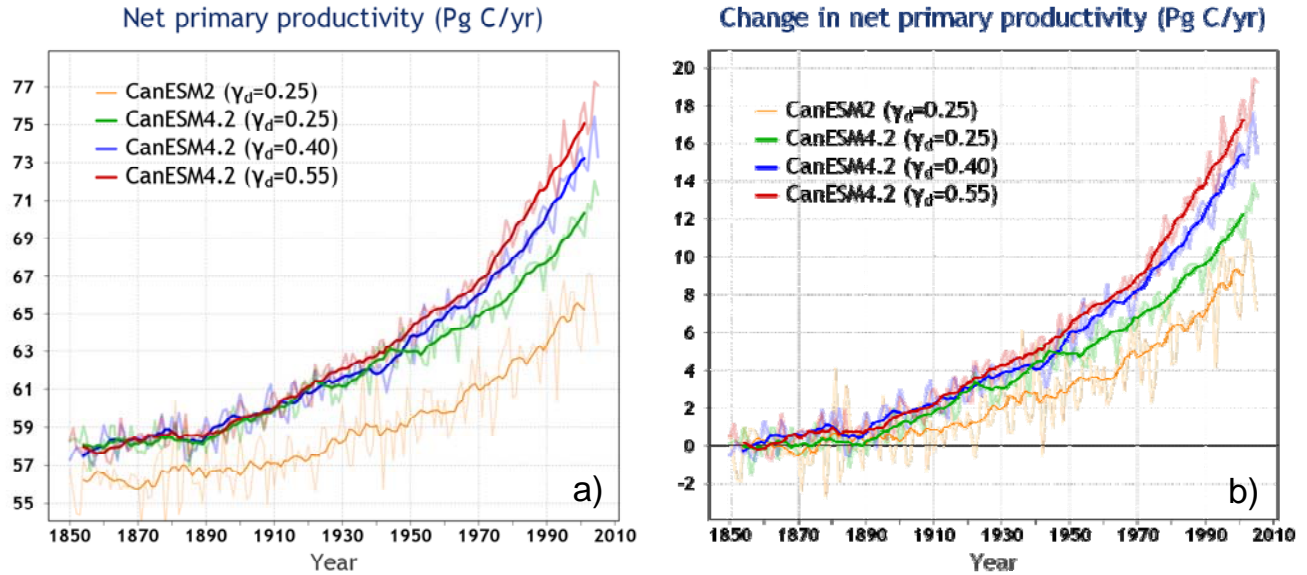
1065

1066

1067

1068

1069



1070

1071 Figure 6: Absolute values of (panel a), and change in (panel b), net primary productivity (NPP)
1072 from CanESM2 and the three CanESM4.2 historical 1850-2005 simulations with different
1073 strengths of the terrestrial CO₂ fertilization effect. The thin lines show the ensemble-mean based
1074 on results from the two ensemble members and the bold lines are their 10-year moving averages.

1075

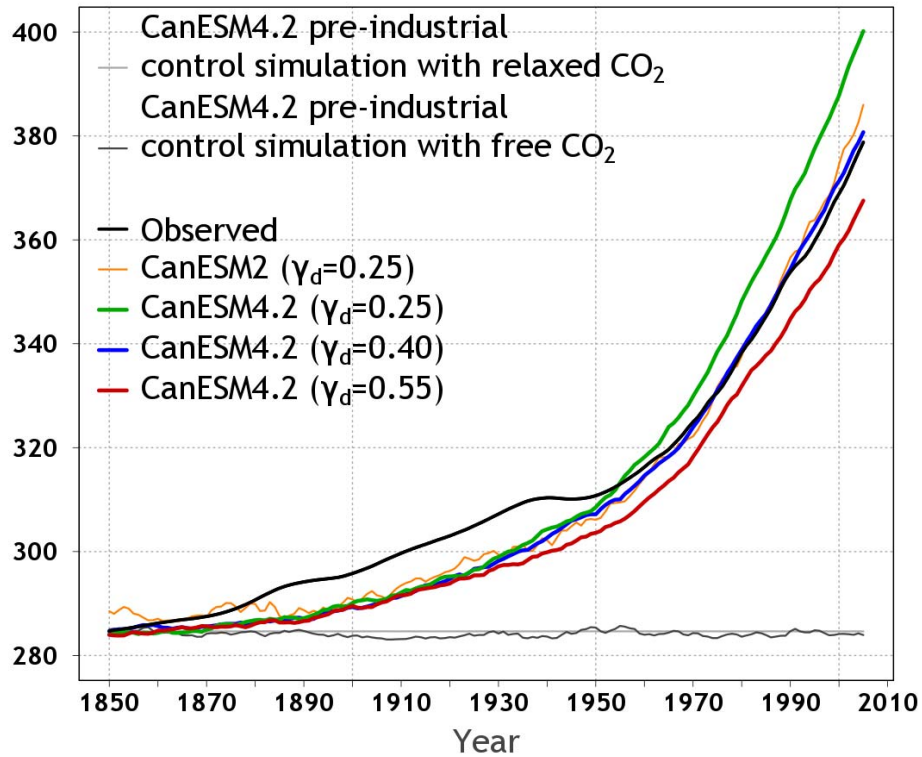
1076

1077

1078

1079

Globally-averaged surface CO₂ concentration (ppm)

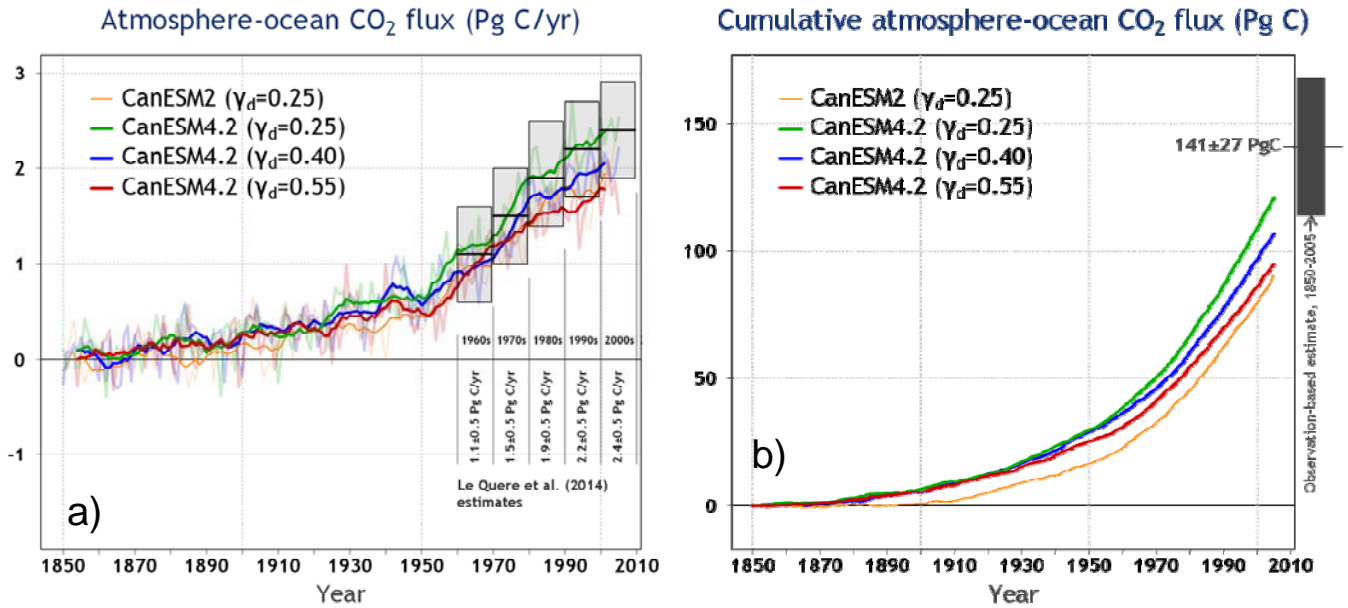


1080

1081 Figure 7: Simulated globally-averaged surface atmospheric CO₂ concentration from CanESM2
1082 and the three CanESM4.2 historical 1850-2005 simulations with different strengths of the
1083 terrestrial CO₂ fertilization effect. The observation-based concentration is shown in black. Also
1084 shown is the CO₂ concentration of 284.6 ppm used in CanESM4.2's pre-industrial simulation in
1085 the relaxed-CO₂ configuration and the simulated concentration from the pre-industrial
1086 CanESM4.2 simulation with interactively determined CO₂.

1087

1088
1089
1090



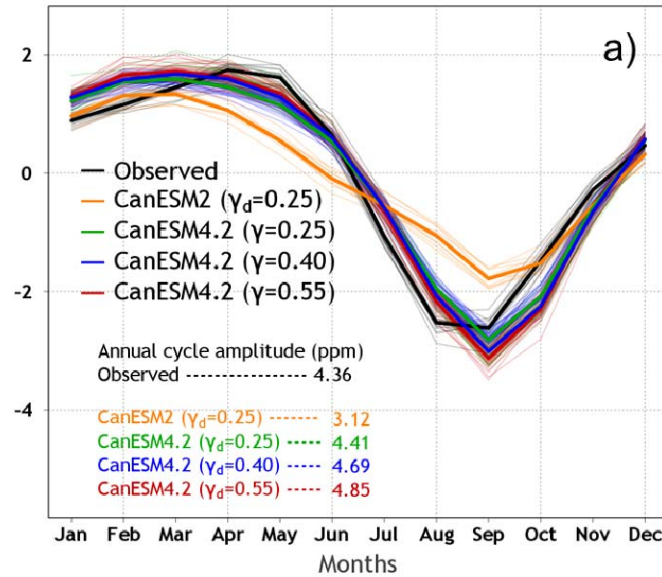
1091

1092 Figure 8: Atmosphere-ocean CO₂ flux (F_O) (panel a) and its cumulative values \tilde{F}_O (panel b) from
1093 CanESM2 and the three CanESM4.2 historical 1850-2005 simulations for three different
1094 strengths of the terrestrial CO₂ fertilization effect. In panel (a) the observation-based estimates of
1095 F_O and their uncertainty, show via boxes, for the decades of 1960, 1970, 1980, 1990 and 2000 are
1096 reproduced from Le Quéré et al. (2015). The bold lines in panel (a) are the 10-year moving
1097 averages of the annual F_L values which are shown in light colours. The results from CanESM2
1098 and CanESM4.2 are the average of the two ensemble members.

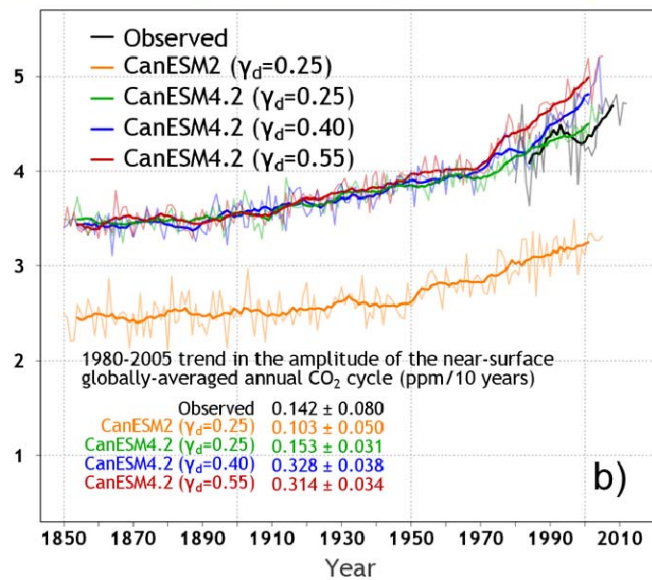
1099

1100

Monthly CO₂ cycle trend-adjusted anomalies (ppm) 1991-2000



Amplitude of the globally-averaged annual CO₂ cycle (ppm)



1101

1102

1103

1104

1105

1106

1107

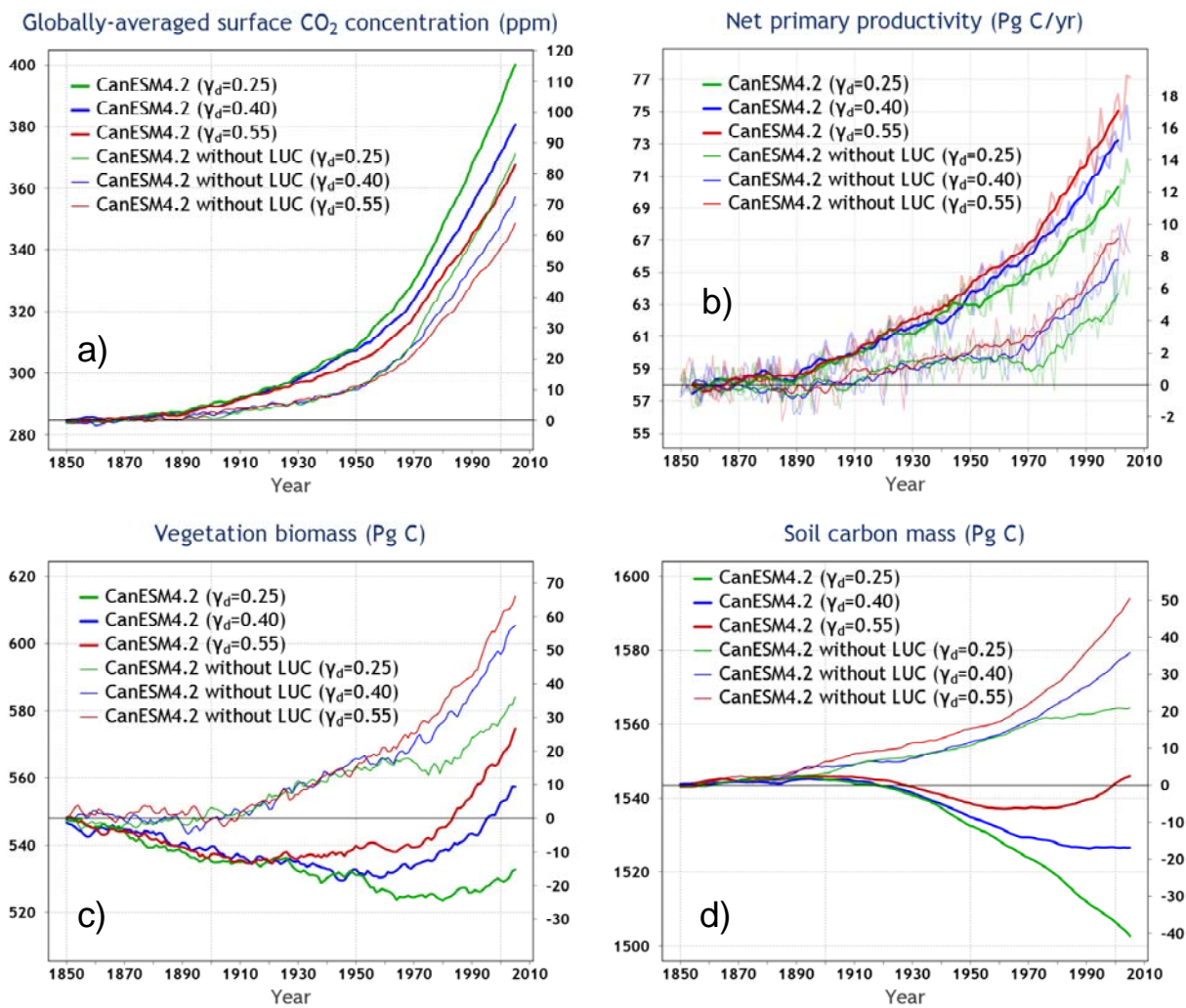
1108

1109

Figure 9: The annual cycle of trend-adjusted globally-averaged near-surface monthly [CO₂] anomalies from CanESM2, the versions of CanESM4.2 for three different strengths of the CO₂ fertilization effect and observation-based estimates for the 1991-2000 period (panel a). Panel (b) shows the time series of the amplitude of the annual cycle of the trend adjusted globally-averaged near-surface monthly [CO₂] anomalies for corresponding model and observation-based estimates. The bold lines are 10-year moving averages and the thin lines for model results are the average of results from two ensemble members.

1110

1111



1112

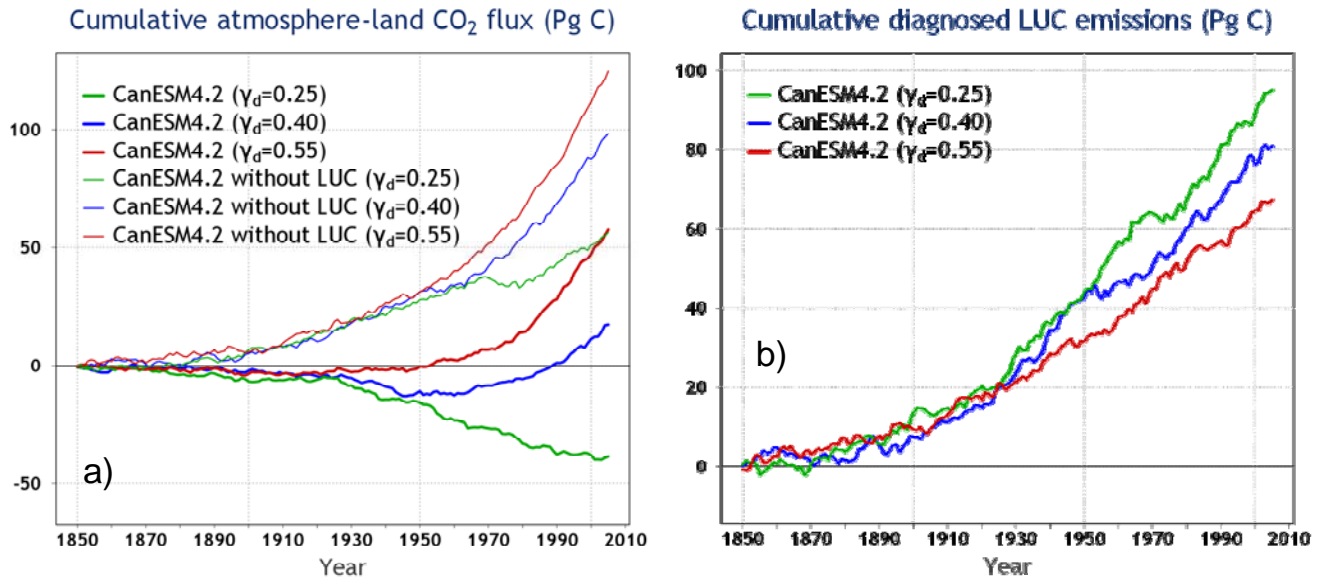
1113 Figure 10: Comparison of CanESM4.2 simulations with and without implementation of
1114 anthropogenic land use change over the historical period for three different strengths of the
1115 terrestrial CO₂ fertilization effect: a) Globally-averaged annual surface atmospheric CO₂
1116 concentration, b) net primary productivity, c) global vegetation biomass, and c) global soil carbon
1117 mass. All lines are the average of results from two ensemble members. Additionally, in panel (b)
1118 the bold lines are the 10-year moving averages.

1119

1120

1121

1122



1123

1124

1125 Figure 11: Comparison of simulated cumulative atmosphere-land CO₂ flux from CanESM4.2
1126 simulations with and without implementation of anthropogenic land use change over the historical
1127 period for three different strengths of the terrestrial CO₂ fertilization (panel a). Panel (b) shows
1128 the cumulative diagnosed LUC emissions calculated using equation (10) as the difference
1129 between cumulative atmosphere-land CO₂ flux from simulations with and without LUC shown in
1130 panel (a). All lines are the average of results from two ensemble members.

1131

1132

1133